Mon. Not. R. Astron. Soc. **000**, ??–?? (2013) Printed 30 January 2015 (MN LATEX style file v2.2)

New Pre-main-Sequence Stars in the Upper Scorpius Subgroup of Sco-Cen

A.C. Rizzuto[1,2], M.J. Ireland[3], A.L. Kraus[1]

[1] *Department of Astronomy, University of Texas, 2515 Speedway, Stop C1400, Austin, Texas 78712, USA*
[2] *Department of Physics and Astronomy, Macquarie University, Sydney NSW, 2109, Australia*
[3] *Research School of Astronomy & Astrophysics, Australian National University, Canberra, ACT 2611, Australia*

30 January 2015

ABSTRACT

We present 237 new spectroscopically confirmed pre-main-sequence K and M-type stars in the young Upper Scorpius subgroup of the Sco-Cen association, the nearest region of recent massive star formation. Using the Wide-Field Spectrograph at the Australian National University 2.3 m telescope at Siding Spring, we observed 397 kinematically and photometrically selected candidate members of Upper Scorpius, and identified new members by the presence of Lithium absorption. The HR-diagram of the new members shows a spread of ages, ranging from ∼3-20 Myr, which broadly agrees with the current age estimates of ∼5-10 Myr. We find a significant range of Li 6708 equivalent widths among the members, and a minor dependence of HR-diagram position on the measured equivalent width of the Li 6708 Å line, with members that appear younger having more Lithium. This could indicate the presence of either populations of different age, or a spread of ages in Upper Scorpius. We also use Wide-Field Infrared Survey Explorer data to infer circumstellar disk presence in 25 of the members on the basis of infrared excesses, including two candidate transition disks. We find that 11.2±3.4% of the M0-M2 spectral type (0.4-0.8 $M_\odot$) Upper Sco stars display an excess that indicates the presence of a gaseous disk.

Key words: stars: pre-main-sequence - stars: formation - open clusters and association: individual: Sco-Cen - surveys - protoplanetary disks

1 INTRODUCTION

The Scorpius-Centaurus-Lupus-Crux Association (Sco OB2, Sco-Cen) is the nearest location to the Sun with recent high-mass star formation (de Zeeuw et al. 1999). Young OB associations, such as Sco-Cen, provide an incredible laboratory in the form of a primordial group of stars directly after formation, which can be exploited in the study of the output of star formation including searches for young exoplanets. The obvious prerequisite for such study is a level of completeness in the identification of association members that is currently not yet attained in Sco-Cen in any mass regime, other than the most massive B-type stars. Sco-Cen contains approximately 150 B-type stars (Rizzuto et al. 2011) which have been typically split into three subgroups: Upper Scorpius, Upper-Centaurus-Lupus (UCL) and Lower-Centaurus-Crux (LCC) with only the B, A and F-type membership of Sco-Cen being considered relatively complete, with some 800 members. Even in this high-mass regime, there is expected to be a ∼30% contamination by interlopers in the kinematic membership selections, mainly due to the lack of precision radial velocity measurements for these objects (Rizzuto et al. 2011). Additionally, in light of the upcoming high-precision GAIA proper motions and parallaxes, a well characterised spectroscopically confirmed Sco-Cen membership will be instrumental in illuminating the substructure of the association.

Unfortunately, Sco-Cen is poorly characterised for its proximity, the reason for which is the enormous area of sky the association inhabits at low Galactic latitudes (∼ $80^\circ \times 25^\circ$ or ∼ 150×50 pc). IMF extrapolation from the high-mass members implies, with any choice of IMF law, that Sco-Cen is expected to have ∼ 10^4 PMS G, K and M-type members, most of which are, as yet, undiscovered. This implies that the vast majority of PMS (<20 Myr) stars in the solar neighbourhood are in Sco-Cen (Preibisch et al. 2002), making Sco-Cen an ideal place to search for young, massive planetary companions. Although some work has been done in illuminating the lower-mass population of Sco-Cen (see Preibisch & Mamajek (2008)), the late-type membership of Sco-Cen cannot be considered complete in any spectral-type or colour range. A more complete picture of the late-type

membership of Sco-Cen is the primary requirement for determining the age spread, structure, and star formation history of the association, for illuminating the properties of star formation, and for embarking on further searches for young exoplanets to better define their population statistics.

The age of the Sco-Cen subgroups has been contentious. Upper Scorpius has long been considered to be ∼5 Myr old, however recent work has shown that it may be as old as 11 Myr (de Geus 1992; Pecaut et al. 2012). Similarly, B, A and F-type UCL and LCC members have main-sequence turn off/on ages of $\sim 16-18$ Myr, while studies of the incomplete sample of lithium-rich G, K and M-type members show a variety of mass-dependent age estimates. The HR-diagram age for the known K-type stars in UCL and LCC is ∼12 Myr, the few known M-type stars indicate a significantly younger age of ∼4 Myr, most likely due to a bias produced by a magnitude limited sample, and the G-type members have an age of ∼17 Myr, which is consistent with the more massive stars (Preibisch & Mamajek 2008; Song et al. 2012). There is also a positional trend in the age of the PMS stars of the older subgroups, with stars closer to the Galactic Plane appearing significantly younger than objects further north. This is almost certainly the result of as yet undiscovered and un-clarified substructure within the older subgroups, which may have a very complex star-formation history.

The above is clear motivation for the identification of the full population of the Sco-Cen association, a task that will require significant observational and computational effort to complete. In this paper, we describe a new search for PMS members of the Upper Scorpius region of the Sco-Cen association. We have used statistical methods to select a sample of likely Upper Scorpius members from all-sky data, and have conducted a spectroscopic survey to determine youth and membership in the Sco-Cen association using the Wide-Field Spectrograph instrument at the Australian National University 2.3 m telescope.

2 SELECTION OF CANDIDATE MEMBERS

We have selected candidate Upper Scorpius members using kinematic and photometric data from UCAC4, 2MASS, USNO-B and APASS (Zacharias et al. 2013; Skrutskie et al. 2006; Monet et al. 2003; Henden et al. 2012). A purely kinematic selection of the low-mass members of Sco-Cen is not sufficient to assign membership to G,K and M-type stars because the quality of the astrometric data available would produce an interloper contamination much higher than would be acceptable for future studies using Sco-Cen as an age benchmark. In order to clearly separate young Upper Scorpius members from field stars, spectroscopic follow-up is needed to identify stellar youth indicators. We employed two separate selection methods to prioritise targets based on kinematic and photometric data.

The first selection used was based on the Bayesian Sco-Cen membership selection of Rizzuto et al. (2011), which uses kinematic and spatial information to assign membership probabilities. We further developed this method to apply to K and M-type stars, in order to properly treat the absence of a parallax measurement. We took the proper-motions from the UCAC4 catalog (Zacharias et al. 2013)

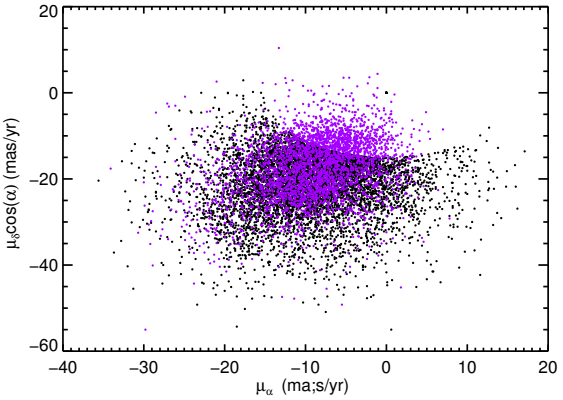

Figure 1. The proper motions of the candidate Upper Scorpius members selected by both the Kraus & Hillenbrand (2007) selection method (black points) and the Bayesian method (purple circles).

and photometry from 2MASS and APASS (Skrutskie et al. 2006; Henden et al. 2012), and used the photometry and a premain-sequence isochrone (Siess et al. 2000) to estimate each candidate member's distance. We then treated the proper-motion and estimated distance together to calculate the membership probability. This selection was magnitude limited, and covered all stars in the UCAC4 catalog with 10<V<16, and comprised of ∼2000 candidate members with membership probability greater than 2%. For a more complete explanation of the Bayesian selection, including information from (Rizzuto et al. 2011) and the changes adopted for use with the K and M-type star data see Appendix A.

The second selection was based on the selection used for the Coma-Ber cluster in the study of Kraus & Hillenbrand (2007), and was designed to select targets for the Upper Scorpius field of the Kepler K2 campaign. Targets which were both placed above the main-sequence based on photometric distance estimates, and had proper-motions consistent with Upper Scorpius membership were deemed to be potential members and included in the observing sample. This selection spanned F to late M-type stars, with targets falling on Kepler silicon prioritized for spectroscopic follow-up. This selection is considerably more conservative than the Bayesian selection, and includes a much larger number of candidates. Where the two selections overlap, we have >90% of the Bayesian selected stars included in the sample. Our final, combined sample was then drawn from both of the above selection; we include a candidate in the final target list if it was identified by either method. Figure 1 displays the proper motions of the selected stars from both samples.

In light of the currently ongoing Galactic Archeology Survey, using the HERMES spectrograph on the Anglo-Ausralian Telescope (Zucker et al. 2012), which will obtain high-resolution optical spectra in the coming years for all stars in the Sco-Cen region of sky, down to V=14, we have decided to primarily observe targets in our sample fainter than this limit. While our selection methods identified candidate Upper Scorpius stars across the entire subgroups ($342^\circ < l < 360^\circ, 10^\circ < b < 30^\circ$) in our observations we strongly favored candidate members which fell upon the Ke-

pler K2 field 2 detector regions, which covers the majority of the centre of Upper-Scorpius with rectangular windows. As such, the spatial distribution of this sample will not reflect the true substructure of Upper Scorpius. We observed all the targets in our K2 sample with Kepler interpolated V magnitudes of ($\sim 13.5 < V_{jk} < 15$), as well as some further brighter targets. In total, we obtained optical spectra for 397 candidate Upper Scorpius K and M-type stars. The full list of observed candidate targets, including both those stars determined to be members and non-members, can be found in Table 1, along with proper motions, computed Bayesian membership probability, integration time, and SNR in the continuum near H-α.

3 SPECTROSCOPY WITH WIFES

The Wide-Field Spectrograph (WIFES) instrument on the Australian National University 2.3m telescope is an integral field, or imaging, spectrograph, which provides a spectrum for a number of spatial pixels across the field of view using an image slicing configuration. The field of view of the instrument is 38×25 arcseconds, and is made up of 25 slitlets which are each one arc second in width, and 38 arcseconds in length. The slitlets feed two 4096×4096 pixel detectors, one for the blue part of the spectrum and the other for the red, providing a total wavelength coverage of 330 - 900 μm, which is dependent on the specific gratings used for the spectroscopy. Each 15 micron pixel corresponds to 1×0.5 arcseconds on sky.

There are a number of gratings offered to observers for use with WiFeS. For identification of Upper Scorpius members, we required intermediate-resolution spectra of our candidate members, with a minimum resolution of ∼3000 at the Li 6708 Å line, and so selected the R7000 grating for the red arm and the B3000 grating for the blue arm, which was used solely for spectral-typing. This provided $\lambda/\Delta\lambda \sim 7000$ spectra covering the lithium 6708Å and H-α spectroscopic youth indicators. A dichroic, which splits the red and blue light onto the two arms of the detector, can be position either at 4800 Å or 5600 Å. For the first three successful observing nights we use the dichroic at 4800 Å which produced a single joined spectrum from 3600 to 7000 AA. For the remaining 7 nights, we position the dichroic at 5600 Å which produces two separate spectra, with the the blue arm covering 3600 to 4800 Å and the red arm covering 5300 to 7000 Å. This change was made to accommodate poor weather backup programs being simultaneously carried out, which will be the subject of future publications. To properly identify members, we required a 3σ-detection of a 0.1Å equivalent width Li line, which corresponds to a signal-to-noise ratio of at least 30 per pixel. In order to achieve this, we took exposures of 5 minutes for R=13 stars (approximately type M3 in Upper Scorpius), and binned by 2 pixels in the y-axis, to create 1×1" spatial pixels and reduce overheads. With overheads we were able to observe 10 targets an hour in bright time, or ∼80-90 targets per completely clear night.

In total we obtained 18 nights of time using WiFeS, split over 2013 and 2014, however the majority of the 2013 nights were unusable due to weather. Our first two observing runs, in June 2013, and April 2014 yielded one half-night of observations each, and our final observing run yielded seven partially clear nights. During our first two nights, we positioned the dichroic at 5500 Å, and during the June 2014 observing run, positioned the dichroic at 4600 Å, which provides more of the red arm, because this mode was deemed better for obtaining radial velocities of B, A and F-type Sco-Cen stars, which we observed as backup targets during poor weather, and will be the subject of a future publication.

4 DATA REDUCTION

The raw WiFeS data was initially reduced with a pre-existing Python data reduction software package called the "WiFeS PyPeline", which was provided to WiFeS observers. The purpose of the software is to transform the CCD image, which consists of a linear spectrum for each spatial pixel of the WiFeS field of view, into a data cube. This involves bias subtraction, flat-fielding, bad pixel and cosmic ray removal, sky subtraction, wavelength calibration, flux calibration, reformatting into the cube structure, and interpolation across each pixel to produce a single wavelength scale for the entire image. On each night, we observed at least one flux standard from Bessell (1999), which are included in the data reduction pipeline as flux calibrator objects. Once this process is complete, the user is left with a single cube for each object observed, with dimensions 25"×38"×3650 wavelength units. For the grating resolutions and angles used in our observations, we obtained spectral coverage from $3200 - 5500$ Å in increments of 1.3 Å in the blue arm, and $5400 - 7000$ Å in increments of 0.78 Å in the red arm.

Following the standard WiFeS reduction procedure, we continued with a further custom reduction, the aim of which was to measure the centroid position of the target object in each wavelength, such that the presence of H-α emitting low-mass stellar companions, outflows, and H-α-bright planetary mass companion could be detected by the measurement of a wavelength-dependent centroid shift. This consisted of determining a best fit point spread function (PSF) model for the spatial image in a clean section of the spectrum, and then measuring the centroid shift of this PSF at each wavelength along the spectrum. An additional benefit of this is a more accurate sky subtraction, and an integrated spectrum of each object, which can be used to measure equivalent widths of key spectral lines. The results of the centroid measurements and any detected companions will be reported in a further publication.

We first cut out a 10" by 10" wide window (10×10 pixels), centered on the target. The vast majority of the stellar flux is contained within the central 3" by 3" region of the windowed image, and so the adopted width of 10" allows a clear region of background around the target; Figure 2b provides an illustration of the data. We then fit a Moffat point spread function (Racine 1996) to a region of the spectral continuum which does not include any spectral features, but is close to the H-α line. This region consisted of 400 spectral units, spanning $6368 - 6544$ Å. Figure 2a displays the spectral region used for the initial PSF fit, as well as the H-α and Li 6708 Å lines for one target in our sample, 1RXS J153910.3-264633, which shows strong indications of youth.

The particular model that we fit to the spatial image is given by;

Table 1. Summary of WiFeS observations of candidate Upper-Scorpius members; the V magnitude provided is either taken from APASS, where available, or interpolated from J and K according to the Kepler K2 instructions. The full table is provided in the online material.

R.A. (J2000.0)	Decl. (J2000.0)	MJD	V (mag)	K (mag)	μ_α (mas)	μ_δ (mas)	Source	P_{mem}	T (sec)	SNR	M?
15 39 06.96	-26 46 32.1	56462	12.5	8.7	-35.3	-41.7	a	31	90	131	Y
15 37 42.74	-25 26 15.8	56462	13.5	9.7	-14.6	-26.7	a	85	90	80	
15 35 32.30	-25 37 14.1	56462	11.7	8.4	-9.0	-22.9	a	69	90	116	
15 41 31.21	-25 20 36.3	56462	10.0	7.2	-16.9	-28.7	a	86	90	151	Y

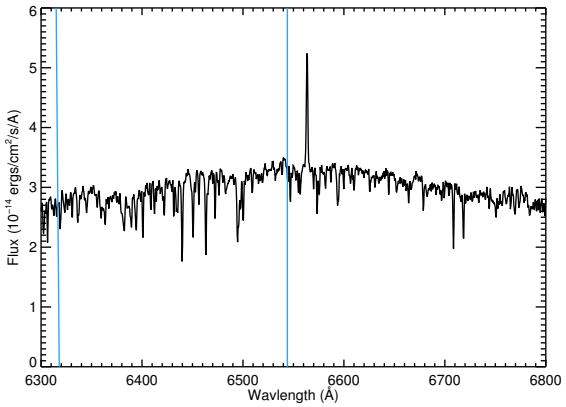

(a)

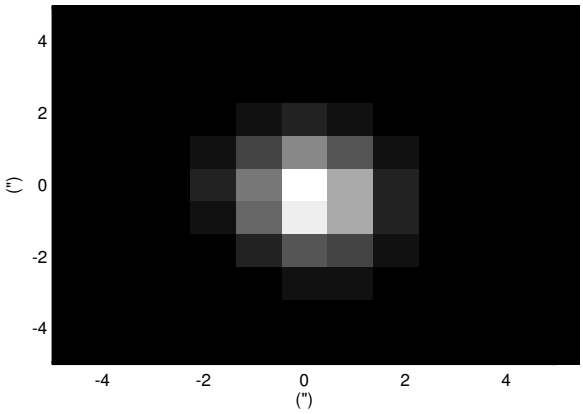

(b)

Figure 2. (a) Example spectrum for object 1RXS J153910.3-264633, a high priority target in our observation sample, which shows signs of youth such as H-α emission and Li 6708Å absorption. The region of the continuum used for the initial PSF fitting is bounded by blue lines. (b) Spatial image created for 1RXS J153910.3-264633 by adding the images at each wavelength of the PSF fitting region of the continuum.

$$\mathrm{PSF} = \mathrm{S} + \mathrm{F}\frac{(2^{\frac{1}{\beta}}-1)(\beta-1)}{\pi w^2(1+(2^{\frac{1}{\beta}}-1)(\theta/w)^2)^\beta}, \qquad (1)$$

where S indicates the sky contribution to the flux, β is an integer parameter that determines the strength of the wings of the Moffat PSF, θ is the distance from the centre of the profile, w is the half width of the Moffat PSF, and F is the stellar flux. Given that we have a two dimensional PSF,

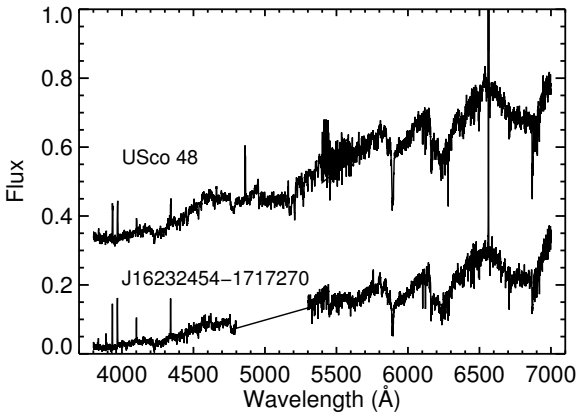

Figure 3. The full WiFeS integrated spectrum produced by first processing with the WiFeS Pypeline, and then our spectro-astrometric analysis for the stars USco 48, a known member of the Upper Scorpius subgroup, and 2MASS J16232454-1717270, high probability candidate, and a new member in identified in our survey. The USco 48 spectrum is an example of the data from the 4800 Å dichroic setup, and the 2MASS J16232454-1717270 spectrum an example of the 5600 Å dichroic setup.

and that each dimension has a different Moffat function half width, we require two different values of w. We create this two dimensional Moffat profile by scaling θ appropriately;

$$\theta = w_x^2(x-x_0)^2 + w_y^2(y-y_0)^2, \qquad (2)$$

where w_x and w_y are the PSF width parameters in each dimension, (x, y) is the position of a given point on the image, and (x_0, y_0) is the image centroid. Inputting this value of θ into a Moffat function with width $w = 1$ will thus produce the desired asymmetric two dimensional profile.

We found that $\beta = 4$, a value which describes most telescope PSFs, yielded the closest fit to our data. We also attempted to fit a Gaussian profile to the spatial images, in the same format as the Moffat profile described in equation 1; however the Gaussian model produced consistently poorer fits to the data than the Moffat model, particularly in the wings of the PSF, with typical values of $\chi_r^2 \sim 4$ for the Gaussian model fit and $\chi_r^2 \sim 2$ for the Moffat model. On the basis of the goodness of fit difference, we adopted the Moffat model exclusively in our analysis. For each target observed, we used the continuum spectral region between 6368−6544 Å to determine the parameters of the Moffat PSF that most closely reproduced the spatial images. We then fixed the half width parameters in each dimension, and fit

our PSF model to each individual wavelength element image along the spectrum to determine S, F and the centroid position for each wavelength. This process provides two useful characteristics, the first of which is the integrated spectrum (F) of the target (see Figure 3), with the sky component (S) subtracted out. Using the cleaned output spectra, we then computed equivalent widths of both the Li 6708 Å and H-α lines for each observed star. The second useful characteristic is the centroid position of the star image at each wavelength interval in the spectrum. This can be used to detect accreting stellar and substellar companions by the measurement of a centroid shift in the H-α line image. An analysis of the centroid positions will be presented in a future publication.

4.1 Spectral Typing

We spectral type the reduced spectra created by the centroid-fitting procedure using spectral template libraries as reference. It is also important to incorporate extinction into the spectral-typing procedure for Upper Scorpius, given the typical values of $0.5 < A_V < 2.0$. If an extinction correction is omitted, spectral typing will produce systematically later spectral types for the members. A combination of two template libraries was chosen for the spectral typing, with spectral types earlier than M0 taken from the Pickles (1998) spectral template library, and the M-type templates taken from the more recent Bochanski et al. (2007).

To carry out the spectral typing, we first computed reduced χ^2 values for each data spectrum on a two-dimensional grid of interpolated template spectra and extinction, with spacing of half a spectral sub-type and 0.1 magnitudes in $E(B-V)$. This was done by first interpolating the template spectra onto the wavelength scale of the data, and then applying the particular amount of extinction according to the Savage & Mathis (1979) extinction law. We also removed the H-α region in the data spectra, because the prevalence of significantly larger H-α emission in young stars will not be adequately reproduced by the templates. The spectral type - extinction point on the grid with the smallest reduced χ^2 was then used as a starting point for least squared fitting with the IDL fitting package MPFIT. The fitting procedure used the same methodology as the grid calculations, with the addition of interpolation between template spectra to produce spectral sub-type models for use in the fitting.

We find the limiting factor in spectral-typing our young Sco-Cen stars to be the fact that the spectral template libraries are built from field stars, and so are not ideal for fitting young, active stars. Hence, while we typically have spectral type fits better than half a spectral sub-type, we report spectral types to the nearest half sub-type, and values of A_V with typical uncertainties of 0.2 magnitudes.

5 THE NEW MEMBERS

Table 2 lists both the Li 6708 Å and Hα equivalent widths, and the estimated spectral types and extinction for the new Upper Sco members, and figure 4 shows the spatial positions of the new members. We have defined a star as an Upper Scorpius member if the measured equivalent width of the Li 6708 Å line was more than $1-\sigma$ above 0.1 Å. While this Li threshold is low, it is significantly larger than the field Li absorption, and is in general keeping with previous surveys. The use of this threshold is further justified given the effects of episodic accretion on Li depletion in the latest models (Baraffe & Chabrier 2010). In general, the vast majority of the identified members have Li 6708 Å equivalent width significantly larger than 0.2 Å and so are bonafide young stars. In total we identify 257 stars as members based on their Li 6708 Å absorption, 237 of which are new.

The proper-motions of the new members, which were calculated from various all-sky catalogs, or taken from the UCAC4 catalog are shown in Figure 4b. The members have proper motions that overlap the Upper Scorpius B, A and F-type members proper motions (blue crosses), although a significantly large spread is seen. This is consistent with the average uncertainty of ∼2-3 mas/yr for the K and M-type proper motions.

Figure 5a displays the Lithium equivalent widths for the identified members as a function of spectral type. The majority of our members are M-type, and we see a sequence of equivalent width with a peak at spectral type M0, and a systematically smaller equivalent width in the M2-M3 range compared to earlier or later M-type members. This is expected as the mid-M range is modelled to show faster Lithium depletion timescale (D'Antona & Mazzitelli 1994).

Interestingly, we also observe a clear spread in the equivalent width of the Lithium 6708Å line. Figure 5b shows the just the M0 to M5 spectral type range. At each spectral type we see a typical spread of ∼0.4 Å in Li equivalent width, and a median uncertainty in the equivalent width measurements of ∼0.03 Å. This implies a ∼10-sigma spread in EW(Li) at each spectral type. Wether or not this spread is caused by an age spread in Upper Scorpius is difficult to determine: we have examined the behaviour of EW(Li) as a function of spatial position, both in equatorial and Galactic coordinate frames and found no significant trend. We note that a similar spread of EW(Li) for M-type Upper Scorpius members was observed by Preibisch et al. (2001). Given the lack of correlation with spatial position, if the EW(Li) spread is caused by an age spread among the members, then the different age populations are overlapping spatially and may not be resolvable without sub-milliarcsecond parallaxes.

In Figure 6, we display the measured H-α equivalent widths for the members. The majority of the PMS members show some level, of H-α emission, with a clear sequence of increasing emission with spectral type. In combination with the presence of Lithium, this is a further indicator of the youth of these objects. Of our 257 members, ∼95% show H-α emission with (1 Å<EW(H-α)<10 Å), and only 11 of the members do not show emission in H-α. All of these 11 members without H-alpha emission are earlier than M0 spectral-type. There are also 35 non-members with H-α emission. Given the values of EW(Hα) for the M-type members we have identified, the majority of them appear to be weak lined T-Tauri stars and ∼10% are Classical T-Tauri stars (CTTS) with EW(Hα) > 10 Å. This proportion agrees with previous studies of Upper-Scorpius members (Walter et al. 1994; Preibisch & Zinnecker 1999; Preibisch et al. 2001), which find a CTTS fraction of between 4 and 10% for K and M-type Upper-Scorpius stars.

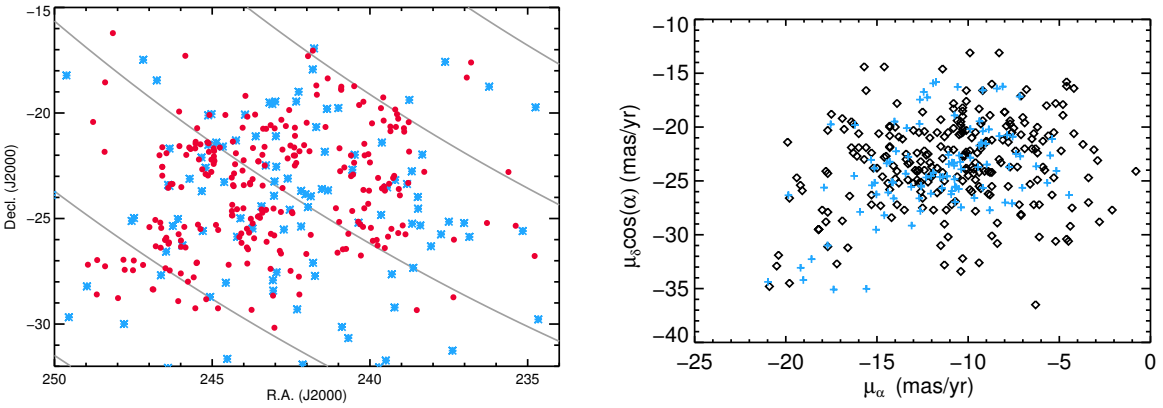

(a) (b)

Figure 4. (a) On-sky positions of the new members (red circles), relative to the B, A and F-type members (blue stars) from Rizzuto et al. (2011). Lines of constant Galactic latitude are shown in grey in steps of 10°, the centre line is $b = 20°$. Note that the apparent substructure seen in the new members is artificially created because we strongly prioritized the Kepler K2 Field 2 detector regions in our survey. (b) The proper motions of the new members (black) and the Hipparcos Upper Scorpius members from Rizzuto et al. (2011) (blue crosses), the typical proper motion uncertainty for our new members is 2-3 mas/yr. There is one new member off-scale at (-35.3,-41.7) mas/yr. Our new members occupy the same region of proper motion space as the established high-mass members.

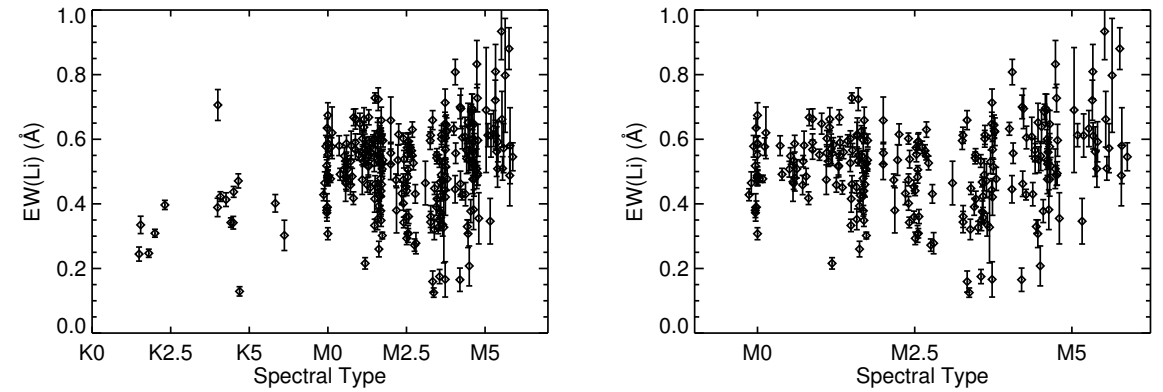

(a) (b)

Figure 5. EW(Li) for the new members. The left panel shows the full K to late M-spread, while the right panel focusses on the M-type range, which shows the largest spread in EW(Li) for a given spectral type.

Table 2. Properties of the Upper Scorpius members identified in our survey. The first column lists our adopted naming system for these new members and the second column lists the 2MASS designation for each of our targets. We also list the the fitted spectral type and visual extinction, and the equivalent widths of the Li 6708Å and Hα lines (EW(Li) and EW(Hα)). The full table is provided in the online material.

Name	2MASS	R.A. (J2000.0)	Decl. (J2000.0)	EW(Li) (Å)	$\sigma_{EW(Li)}$ (Å)	EW(Hα) (Å)	$\sigma_{\mathrm{EW(H}_\alpha)}$ (Å)	SpT	A_V (mag)
RIK-1	J15390696-2646320	15 39 06.96	-26 46 32.1	0.46	0.02	-1.22	0.03	M0.5	0.2
RIK-2	J15413121-2520363	15 41 31.21	-25 20 36.3	0.40	0.01	-2.70	0.04	K2.5	0.1
RIK-3	J15422621-2247458	15 42 26.21	-22 47 46.0	0.46	0.04	-3.08	0.07	M1.5	0.3
RIK-4	J15450970-2512430	15 45 09.71	-25 12 43.0	0.61	0.02	-2.02	0.04	M1.5	0.4

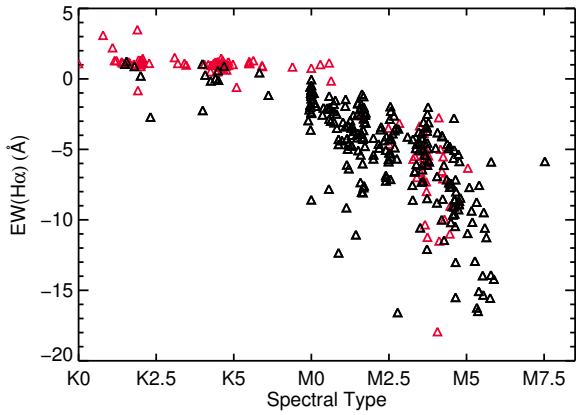

Figure 6. EW(H−α) for the new members (black) and the non-members (red). The members follow a clear sequence with H-α increasing with spectral-type. In the K spectal types, we see that non-members show H-α absorption which is generally stronger than that seen in the members, some of which show weak emission.

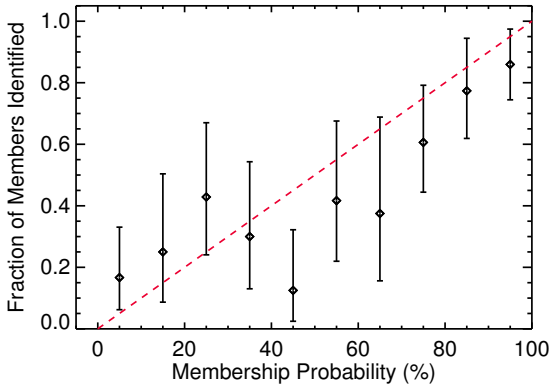

Figure 7. Fraction of stars identified as members plotted against membership probability computed with our Bayesian selection algorithm. The red line represents the ideal fraction of detected members. We see a very close agreement between the computed membership probability and the fraction of stars which were confirmed as members.

6 THE EFFICIENCY OF THE BAYESIAN SELECTION ALGORITHM

The selection methods we have used to create our target list provide a significant improvement of member detection rate when compared to what can be achieved from simple color-magnitude cuts. We see a large overall identification rate of ∼65% for our sample of observed stars. Using the membership probabilities computed for the stars we have observed, we expected that 73±7% of the observed stars would be members, which agrees with the observed members fraction of 68%. We also find that as a function of computed membership probability, the fraction of members identified among the sample behaves as expected. Figure 7 displayed the membership fraction as a function of probability.

Given that our probabilities have been empirically verified to provide a reasonable picture of Upper Scorpius membership, we can derive an estimate for the expected number of M-type members in the subgroup by summation of the probabilities. We find that the total expected number of Upper Scorpius members in the ∼0.2 to 1.0 $M_\odot$ range, or late-K to ∼M5 spectral type range, is ∼2100±100 members. This agrees with initial mass function estimates which indicate that there are ∼1900 members with masses smaller than 0.6 $M_\odot$ in Upper Scorpius (Preibisch et al. 2002).

7 THE HR-DIAGRAM OF THE MEMBERS

With the spectral types and extinctions we have determined for the members using the Bochanski et al. (2007) and Pickles (1998) spectral libraries, we can place them on a HR-diagram in the model parameter space. There is significant variability in synthesized photometry between different models for PMS stars, making comparison in the color-magnitude space difficult. Furthermore, the most reliable magnitudes for M-type stars are the near-IR 2MASS photometry, which show minimal variation in the M-type regime where the PMS is near vertical. Instead, we use the spectral types and the empirical temperature scale and J-band bolometric corrections for 5-30 Myr stars produced by Pecaut & Mamajek (2013) and we further correct for extinction using our fitted values of A_V from the spectral typing process, and the Savage & Mathis (1979) extinction law. The resulting HR diagram can be seen in Figure 8. We have also superimposed five BT-Settl (Allard et al. 2011) isochrones of ages 1, 3, 5, 10 and 20 Myr onto the HR-diagram at the typical Upper Scorpius distance of 140 pc (Rizzuto et al. 2011). These particular models were chosen because they were used by Pecaut & Mamajek (2013) in the generation of their temperature scale, and so any relative systematic differences between the models and the temperature scale will most likely be minimized.

Upon initial inspection, it appears that for a given temperature range, the Upper Scorpius members inhabit a significant spread of bolometric magnitudes. This is most likely highly dominated by the distance spread of the Upper Scorpius subgroup, which has members at distances between 100 and 200 pc, corresponding to a spread in bolometric magnitude of ∼1.5 mag between the nearest and furthers reaches of Upper Scorpius. Using the distance distribution of the Rizzuto et al. (2011) high-mass membership for Upper Scorpius, we find that the expected spread in bolometric magnitude due to distance which encompasses 68% of members is approximately +0.33 and −0.54 magnitudes. Similarly, unresolved multiple systems can bias the sample towards appearing younger by an increase in bolometric magnitude of up to ∼0.7 mags for individual stars.

In the later spectral types, beyond $\log T_{\rm eft} = 3.52$ we also begin to see the effects of the magnitude limit of our survey, which operated primarily in the range 13.5 <V< 15 and so only the brightest, and hence nearest and potentially youngest late M-type members in our original target list were identified, although significant Li depletion at these temperatures is not expected to occur until ages beyond 50 Myr. Even with distance spread blurring the PMS in Upper Scorpius, we can see that most of the members appear

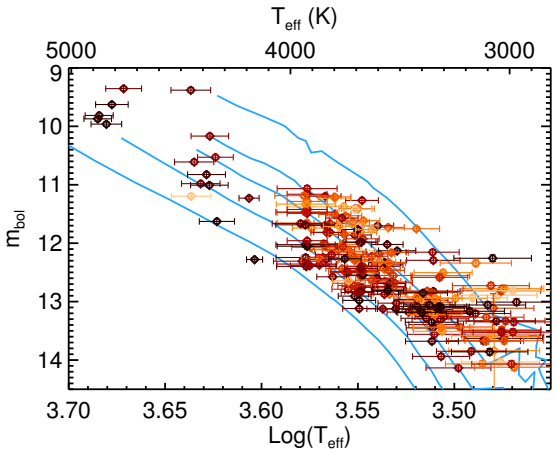

Figure 8. HR diagram for the Upper Scorpius members we have identified, with bolometric corrections and effective temperatures taken from the Pecaut & Mamajek (2013) young star temperature-color scale. The blue lines are the BT-Settl isochrones (Allard et al. 2011) of ages 1, 3, 5, 10 and 20 Myr placed at the typical distance to Upper Scorpius of 140 pc. The color of each point indicates the measured EW(Li) for the star, with darker color indicating a lower EW(Li). The color range spans 0.3 <EW(Li)< 0.7 linearly, with values outside this range set to the corresponding extreme color. The uncertainties are determined by the accuracy of our spectral typing methods, which is typical half a spectral sub-type.

to be centered around the 5-10 Myr age range in the earlier M-type members.

We have also indicated the measured EW(Li) values for the members on the HR-diagram as a color gradient, with darker color indicating a smaller EW(Li). The scale encompasses a range of 0.3 <EW(Li)< 0.7 Å, with values outside this range set to the corresponding extreme color. There is a marginal positional dependence of HR-diagram position with EW(Li): we see that, in particular for the earlier M-type members, the larger values of EW(Li) (light orange) are more clustered around the 3-5 Myr position, while the smaller values of EW(Li) (dark red) are clustered closer to 5-10 Myr. This could indicate the presence of a spread of ages, or populations of different age in the Upper Scorpius subgroup.

There is some other evidence of different age populations in the Upper Scorpius subgroup: The existence of very young B-type stars, such as τ-Sco, and ω-Sco which have well measured temperatures and luminosities that indicate an age of ∼2-5 Myr (Simón-Díaz et al. 2006) support a young population in Upper Scorpius. The B0.5 binary star δ-Sco is also likely to be quite young (∼5 Myr) (Code et al. 1976). Pecaut et al. (2012) place it on the HR diagram at and age of ∼10 Myr, however, due to the rapid rotation and possible oblate spheroid nature of the primary, the photometric prescriptions for determining the effective temperature and reddening of the primary used by Pecaut et al. (2012) are likely to fail for this object. The spectral type is more consistent with a temperature of ∼30000 K. Additionally, the presence of other evolved B-type stars is evidence for an older population (Pecaut et al. 2012). Furthermore, the recent age estimate of 13 Myr for the F-type members of Upper Scorpius by Pecaut et al. (2012) further supports an older population in the subgroup. If the HR diagram position on EW(Li) that we observe among our members is real than this also supports multiple age population in Upper Scorpius.

8 DISK CANDIDATES

We have also obtained the Wide-Field Infrared Survey Explorer (WISE) infrared photometry (Wright et al. 2010), from the ALLWISE version of the catalog, for the observed candidate members in order to determine the prevalence of circumstellar disks among our new members. The identification of new populations of stars bearing disks is valuable because it provides extension to the current samples used in the study of disk property measurements and disk evolution. The AllWISE catalog provides photometry in four bands W1, W2, W3 and W4, with effective wavelengths of 3, 4.5, 12 and 22 μm respectively. The W2 and W3 photometry is effective for tracing the presence of an inner disk, while excess in the W4 band photometry can indicate the presence of a colder, outer disk or transitional disk.

We queried the ALLWISE catalog for the positions of the 397 stars we observed from our sample, including 237 new members, with a search radius of 5". The search returned 395 matches with varying levels of photometric quality. We then placed each star on three spectral type-color diagrams incorporating 2MASS (Skrutskie et al. 2006) K-band photometry, these were K-W2, K-W3, and K-W4. Past studies have used both K, and W1 as the base photometry for building color-color diagrams (Carpenter et al. 2006, 2009; Rizzuto et al. 2012; Luhman et al. 2010; Luhman & Mamajek 2012). Typically, the presence of a disk within ∼ 3 AU of a host star increases the brightness in the IR wavelengths, with ∼5 μm being the approximate wavelength where the disk dominates in brightness. Both the W1 and K magnitudes are long enough such that reddening is not a significant issue, but also shorter than the expected point of disk domination. We found that examining the WISE bands relative to the K magnitude produced a better separation of disk bearing stars from photospheric emission, and so we report the analysis in terms of this methodology.

Figure 9 displays the three spectral type-color diagrams. We excluded any WISE photometry in a given band that was flagged as having a signal to noise ratio of < 4, as a non-detection, or flagged as being contaminated by any type of image artifact in the catalog. This resulted in the exclusion of 56, 10 and 312 objects in the W2, W3, and W4 bands respectively. The primary source of the exclusions for the W4 band was non-detection or low signal to noise at 22 μm, and most of the exclusions in the W2 and W3 bands were due to contamination by image artifacts. To reduce contamination by extended sources we also excluded any object flagged as being nearby a known extended source or with significantly poor photometry fits, there were eight such objects. The WISE band images for these stars were then inspected visually to gauge the extent of contamination. We found the three of the objects were not significantly effected by the nearby extended source, and so included them in the analysis. After excluding these objects we were left with 333, 379 and 77 objects with photometry of sufficient quality in the W2, W3 and W4 bands respectively.

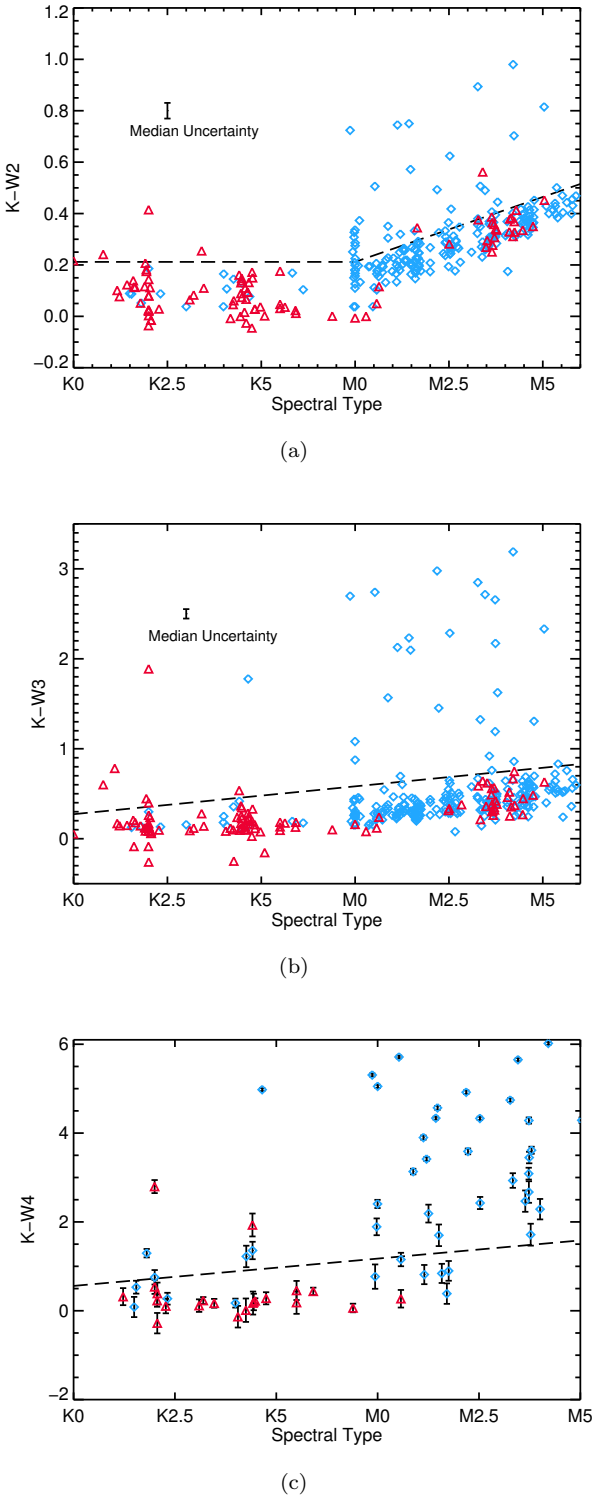

Figure 9. Near IR and WISE band color-color diagrams for both the newly identified members (blue diamonds) and non-members (red triangles) from our spectroscopic survey for $(J-K, K-W2)$, $(J-K, K-W3)$, and $(J-K, K-W4)$. We have omitted objects in each WISE band that were flagged as having poor or contaminated photometry in the catalog. The dashed lines indicate the position of the upper boundary of the photospheric sequence. If a star is above this threshold we designate it as displaying an excess in the particular band.

Due to the age of Upper Scorpius of ∼10 Myr, the majority of members no longer possess a disk, providing sufficient numbers of stars to clearly identify photospheric emission. Hence the photosphere color can be determined from the clustered sequence in the spectral type-color diagrams. We fit a straight lines in the K-W3 and K-W4 WISE band colors, and a disjointed line in K-W2, and then place a boundary where the photospheric sequence ends. For K-W3 the boundary line is given by the points (K0,0.27) and (M5,0.8) and for K-W4 the points (K0,0.56) and (M5,1.6).The sloped part of the boundary line for K-W2 is defined by the points (M0,0.21) and (M5,0.46), and the flat section by K-W2 = 0.21, for spectral types earlier than M0. These boundaries are shown as black lines in Figures 9. Stars with color redder than these boundaries we deem to display an excess in the particular WISE band. Upon inspection, we find that our placement of the end of the photospheric sequence is closely consistent with that of (Luhman & Mamajek 2012). In the K-W4 color, we find that for stars of spectral type later than ∼M2, the photospheric emission in W4 is undetectable by WISE.

For those stars which displayed excesses in any combination of WISE bands, we visually inspected the images to exclude the possibility that the excesses could have been caused by the presence of close companions or nebulosity. We also found that in a few cases background structure in the W4 image could cause the appearance of an excess, although this effect was largely mitigated by our signal-to-noise cutoff. We rejected 23 of the excess detections after inspection, 12 of which were caused by background structure or nearby nebulosity, and 11 of which were due to blending with nearby stars. We further excluded any object which shows an excess in only the K-W2 color as likely being produced by unresolved multiplicity. After these rejections, 27 stars remained with reliable excess detections. Additionally, a single object, 2MASS J16194711-2203112 , displayed an excess in K-W3, but had a W4 detection with signal-to-noise of 3.5. Upon inspection of the corresponding W4 band image, we included it as exhibiting an excess in K-W4.

We can classify the disk types by the amount of excess displayed in different colors compared to the photosphere. We adopt disk type criteria in the E(K-W4), E(K-W3) space consistent with those described in Luhman et al. (2010) and Luhman & Mamajek (2012), which identify four different categories of disk: Full or primordial disks, transition disks, evolved disks, and debris or evolved transition disks. Primordial or full disks exhibit strong emission across the entire IR spectral range. Transition disks are structurally different in that they have a significant cleared inner hole, which is visible as a weaker emission at the shorter IR wavelengths, but still relatively bright in the longer IR wavelengths. Evolved disks do not show a gap in IR emission, but have started to become thinned and appear fainter at all IR wavelengths than unevolved full disks, with a steady decline in IR excess with age (Carpenter et al. 2009). Debris disk and evolved transition disk have similar IR SED's, showing only weak excesses at the longer IR wavelengths. Figure 10b show both E(K-W4) and E(K-W3) for the stars identified as having displaying an excess. The lines in Figure 10b bound the different regions populated by the various disk types. We classify all objects with excesses in W3 and W4 beneath the dashed line to be debris or evolved transition disks candidates, and

2MASS	R.A. (J2000.0)	Decl. (J2000.0)	M	E	D	W2	W3	W4
15581270-2328364	15 58 12.70	-23 28 36.4	Y	XXE	D/ET	7.97	7.88	6.72
15573430-2321123	15 57 34.31	-23 21 12.3	Y	EEE	E	8.67	8.30	5.58
16052157-1821412	16 05 21.57	-18 21 41.2	Y	XEE	T	7.24	6.36	3.16
16064385-1908056	16 06 43.86	-19 08 05.5	Y	EEE	E	8.86	8.11	6.79
16064794-1841437	16 06 47.94	-18 41 43.8	Y	XEE	T	8.75	8.10	3.93
16120668-3010270	16 12 06.68	-30 10 27.1	Y	EEE	F	8.81	6.58	3.60
16134781-2747340	16 13 47.82	-27 47 34.0	Y?	XEE	E	7.93	7.81	7.04
15594426-2029232	15 59 44.27	-20 29 23.4	Y	EEE	F	9.59	8.07	6.12
16120505-2043404	16 12 05.05	-20 43 40.5	Y	EEE	E	8.71	7.50	5.93
16112601-2631558	16 11 26.03	-26 31 55.9	Y	XEE	E	9.24	8.12	5.98
16093164-2229224	16 09 31.66	-22 29 22.4	Y	EEE	F	8.65	6.17	4.23
16252883-2607538	16 25 28.81	-26 07 53.8	Y	XXE	D/ET	9.61	9.24	7.43
16333496-1832540	16 33 34.97	-18 32 53.9	Y	XEE	E	9.81	9.21	7.72
16023587-2320170	16 02 35.89	-23 20 17.1	Y	XEE	E	9.79	8.31	7.41
16011398-2516281	16 01 13.99	-25 16 28.2	Y	EEE	E	9.97	8.79	6.81
16132190-2136136	16 13 21.91	-21 36 13.7	Y	EEE	F	9.40	7.88	5.41
16194711-2203112	16 19 47.12	-22 03 11.2	Y	XEX	E	10.13	9.24	
16041893-2430392	16 04 18.93	-24 30 39.3	Y	EEE	F	8.23	6.57	4.52
16100501-2132318	16 10 05.02	-21 32 31.9	Y	EEE	F	8.23	6.25	3.64
16200616-2212385	16 20 06.16	-22 12 38.5	Y	XEE	E	10.12	8.48	7.20
15564244-2039339	15 56 42.45	-20 39 34.2	Y	EEE	F	9.79	7.57	4.63
16271273-2504017	16 27 12.74	-25 04 01.8	Y	EEE	F	8.64	7.25	5.48
15583620-1946135	15 58 36.20	-19 46 13.5	Y	EEE	F	9.74	7.53	4.70
16012902-2509069	16 01 29.03	-25 09 06.9	Y	EEE	F	9.19	7.24	5.34
16071403-1702425	16 07 14.02	-17 02 42.7	Y	XEE	F	10.25	8.10	6.47
16145244-2513523	16 14 52.41	-25 13 52.4	Y	EEE	E	9.95	9.13	7.52
16153220-2010236	16 15 32.20	-20 10 23.7	Y	EEE	F	8.16	6.68	4.57

Table 3. List of stars in our sample with observed IR excesses in the WISE bands. (M) indicates the membership status of the star, (E) list the detection of IR excesses in the three WISE bands, (D) labels the candidate disk classification where F, E, T and D/ET mean full, evolved, transition, and debris or evolved transition respectively. The final three columns list the availability of photometry in the three longest WISE bands. The question mark (?) indicates the star HD-145778, which is likely to be an F-type members of Upper Scorpius.

the objects above the solid line to be full disks. Stars with excess between these two lines we classify as evolved disk candidates. Finally, we identify the two objects with a large W4 excess, but W3 excesses too small to be classified as full disks, as transition disk candidates. Table 3 lists the excess status for the stars with detected excesses.

In total, we identify 26 of the Upper Scorpius members as displaying a disk-indicating excess with spectral types later than K0, and one star without significant Lithium absorption that also displays an excess. This latter object is an F4.5 spectral type object,, HD-145778, with $EW(Li) = 0.09 \pm 0.2$. The presence of some Lithium absorption, combined with the disk presence mean that this object can be considered to be a member of Upper Scorpius. We have included it as a member at the end of Table 2. HD-145778 is not in this HIPPARCOS catalog (Perryman et al. 1997), potentially explaining why it was not included in past memberships.

Due to the WISE detection limit in the W4 band, we are almost certainly not able to identify the vast majority of the evolved transitional and debris disks, which show only a small color excess in K-W4. Indeed, we only detect two such disks in our sample, one of which, USco 41, was previously identified with Spitzer photometry (Carpenter et al. 2009), when significantly more are expected from previous statistics (Carpenter et al. 2009; Luhman & Mamajek 2012). Furthermore, it is likely that a number of evolved disks around stars of spectral type later than ∼M3 are not detected here. For this reason it is difficult to meaningfully estimate the disk or excess fraction for our entire sample. In the M0 to M2 spectral type range, where we expect the majority of the full, evolved and transitional disks to be detectable by WISE, we have 11 disks, 6 of which are full, 4 evolved and 1 transitional. Excluding all those members flagged for extended emission, confusion with image artifacts, or unreliable excesses, we find and excess fraction of 11.2±3.4%. Carpenter et al. (2009) found a primordial disk fraction for M-type Upper Scorpius members of ∼17%, and Luhman & Mamajek (2012) find excess fractions of 12% and 21% for K-type and M0 to M4-type members respectively. Given the strong increase in excess fraction towards the late M-type members and the potential for some missed evolved disks due to the WISE detection limits, we find that our excess fraction estimate is consistent with these past results.

9 CONCLUSIONS

We have conducted a spectroscopic survey of 397 candidate Upper Scorpius association K and M-type members chosen through statistical methods, and revealed 237 new PMS members among the sample based on the presence of Li absorption. We also identify 25 members in our sample with WISE near-infrared excesses indicative of the presence of a circumstellar disk, and classify these disk on the basis of their color excess in different WISE bands. We find that

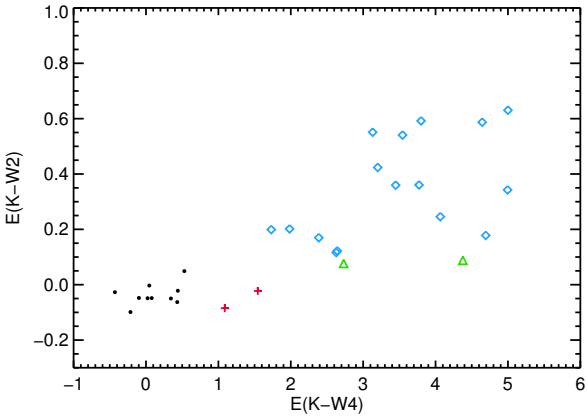

(a)

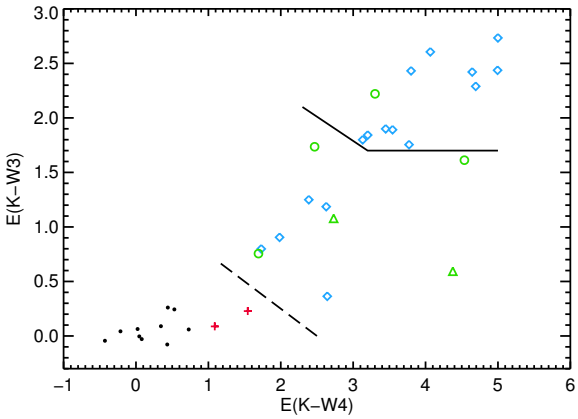

(b)

Figure 10. Excesses in K-W2 vs. K-W4 and K-W3 vs. K-W4 for the members observed in our survey. The plots includes members with out excess (black circles), with excesses in W2, W3 and W4 (blue diamonds), with excesses in the two longest WISE bands with and without reliable W2 photometry (green triangles and circles respectively), and members with an excess in only the W4 band (red plusses). We also include three members with just W3 excesses, which were detected in W4, but without excesses which clearly sit above the diskless sequence (purple squares). The black lines indicate adopted boundaries for different disk classifications.

the members show a significant spread in EW(Li), and upon placing the members on a HR diagram, we find that there is a potential age spread, with a small correlation between EW(Li) and HR-diagram position. This could indicate the presence of a distribution of ages, or multiple populations of different age in Upper Scorpius.

REFERENCES

Allard F., Homeier D., Freytag B., 2011, in Astronomical Society of the Pacific Conference Series, Vol. 448, 16th Cambridge Workshop on Cool Stars, Stellar Systems, and the Sun, Johns-Krull C., Browning M. K., West A. A., eds., p. 91

Baraffe I., Chabrier G., 2010, A&A, 521, A44

Bessell M. S., 1999, PASP, 111, 1426

Bochanski J. J., West A. A., Hawley S. L., Covey K. R., 2007, AJ, 133, 531

Carpenter J. M., Mamajek E. E., Hillenbrand L. A., Meyer M. R., 2006, ApJ, 651, L49

—, 2009, ApJ, 705, 1646

Code A. D., Bless R. C., Davis J., Brown R. H., 1976, ApJ, 203, 417

D'Antona F., Mazzitelli I., 1994, ApJS, 90, 467

de Geus E. J., 1992, A&A, 262, 258

de Zeeuw P. T., Hoogerwerf R., de Bruijne J. H. J., Brown A. G. A., Blaauw A., 1999, AJ, 117, 354

Henden A. A., Levine S. E., Terrell D., Smith T. C., Welch D., 2012, Journal of the American Association of Variable Star Observers (JAAVSO), 40, 430

Kraus A. L., Hillenbrand L. A., 2007, AJ, 134, 2340

Kraus A. L., Ireland M. J., Martinache F., Hillenbrand L. A., 2011, ApJ, 731, 8

Luhman K. L., Allen P. R., Espaillat C., Hartmann L., Calvet N., 2010, ApJS, 186, 111

Luhman K. L., Mamajek E. E., 2012, ApJ, 758, 31

Monet D. G., Levine S. E., Canzian B., Ables H. D., Bird A. R., Dahn C. C., Guetter H. H., Harris H. C., Henden A. A., Leggett S. K., Levison H. F., Luginbuhl C. B., Martini J., Monet A. K. B., Munn J. A., Pier J. R., Rhodes A. R., Riepe B., Sell S., Stone R. C., Vrba F. J., Walker R. L., Westerhout G., Brucato R. J., Reid I. N., Schoening W., Hartley M., Read M. A., Tritton S. B., 2003, AJ, 125, 984

Pecaut M. J., Mamajek E. E., 2013, ApJS, 208, 9

Pecaut M. J., Mamajek E. E., Bubar E. J., 2012, ApJ, 746, 154

Perryman M. A. C., Lindegren L., Kovalevsky J., Hoeg E., Bastian U., Bernacca P. L., Crézé M., Donati F., Grenon M., van Leeuwen F., van der Marel H., Mignard F., Murray C. A., Le Poole R. S., Schrijver H., Turon C., Arenou F., Froeschlé M., Petersen C. S., 1997, A&A, 323, L49

Pickles A. J., 1998, PASP, 110, 863

Preibisch T., Brown A. G. A., Bridges T., Guenther E., Zinnecker H., 2002, AJ, 124, 404

Preibisch T., Guenther E., Zinnecker H., 2001, AJ, 121, 1040

Preibisch T., Mamajek E., 2008, The Nearest OB Association: Scorpius-Centaurus (Sco OB2), Astronomical Society of the Pacific, pp. 235–+

Preibisch T., Zinnecker H., 1999, AJ, 117, 2381

Racine R., 1996, PASP, 108, 699

Rizzuto A. C., Ireland M. J., Robertson J. G., 2011, MNRAS, 416, 3108

Rizzuto A. C., Ireland M. J., Zucker D. B., 2012, MNRAS, 421, L97

Robin A. C., Reylé C., Derrière S., Picaud S., 2003, A&A, 409, 523

Savage B. D., Mathis J. S., 1979, ARA&A, 17, 73

Siess L., Dufour E., Forestini M., 2000, A&A, 358, 593

Simón-Díaz S., Herrero A., Esteban C., Najarro F., 2006, A&A, 448, 351

Skrutskie M. F., Cutri R. M., Stiening R., Weinberg M. D., Schneider S., Carpenter J. M., Beichman C., Capps R., Chester T., Elias J., Huchra J., Liebert J., Lonsdale C., Monet D. G., Price S., Seitzer P., Jarrett T., Kirkpatrick J. D., Gizis J. E., Howard E., Evans T., Fowler J., Fullmer L., Hurt R., Light R., Kopan E. L., Marsh K. A., McCal-

lon H. L., Tam R., Van Dyk S., Wheelock S., 2006, AJ, 131, 1163

Song I., Zuckerman B., Bessell M. S., 2012, AJ, 144, 8

Steinmetz M., Zwitter T., Siebert A., Watson F. G., Freeman K. C., Munari U., Campbell R., Williams M., Seabroke G. M., Wyse R. F. G., Parker Q. A., Bienaymé O., Roeser S., Gibson B. K., Gilmore G., Grebel E. K., Helmi A., Navarro J. F., Burton D., Cass C. J. P., Dawe J. A., Fiegert K., Hartley M., Russell K. S., Saunders W., Enke H., Bailin J., Binney J., Bland-Hawthorn J., Boeche C., Dehnen W., Eisenstein D. J., Evans N. W., Fiorucci M., Fulbright J. P., Gerhard O., Jauregi U., Kelz A., Mijović L., Minchev I., Parmentier G., Peñarrubia J., Quillen A. C., Read M. A., Ruchti G., Scholz R., Siviero A., Smith M. C., Sordo R., Veltz L., Vidrih S., von Berlepsch R., Boyle B. J., Schilbach E., 2006, AJ, 132, 1645

Walter F. M., Vrba F. J., Mathieu R. D., Brown A., Myers P. C., 1994, AJ, 107, 692

Wright E. L., Eisenhardt P. R. M., Mainzer A. K., Ressler M. E., Cutri R. M., Jarrett T., Kirkpatrick J. D., Padgett D., McMillan R. S., Skrutskie M., Stanford S. A., Cohen M., Walker R. G., Mather J. C., Leisawitz D., Gautier III T. N., McLean I., Benford D., Lonsdale C. J., Blain A., Mendez B., Irace W. R., Duval V., Liu F., Royer D., Heinrichsen I., Howard J., Shannon M., Kendall M., Walsh A. L., Larsen M., Cardon J. G., Schick S., Schwalm M., Abid M., Fabinsky B., Naes L., Tsai C.-W., 2010, AJ, 140, 1868

Zacharias N., Finch C. T., Girard T. M., Henden A., Bartlett J. L., Monet D. G., Zacharias M. I., 2013, AJ, 145, 44

Zucker D. B., de Silva G., Freeman K., Bland-Hawthorn J., Hermes Team, 2012, in Astronomical Society of the Pacific Conference Series, Vol. 458, Galactic Archaeology: Near-Field Cosmology and the Formation of the Milky Way, Aoki W., Ishigaki M., Suda T., Tsujimoto T., Arimoto N., eds., p. 421

APPENDIX A: BAYESIAN SELECTION OF CANDIDATE PMS UPPER SCORPIUS STARS

The Bayesian selection method we have employed to identify candidate Upper Scorpius members in the low-mass (K and M-type) regime is largely based upon the high-mass star selection of Rizzuto et al. (2011), with some significant changes to accommodate the particular data available for the low-mass stars. As in Rizzuto et al. (2011) we consider two models: (1) The Upper Scorpius group model (M_g) and (2) the field model describing ordinary field stars (M_f). These models both provide a variety of information, including position, distance and velocity distributions. For use with the low-mass stars, we also include a model isochrone;

$$M_{g,f}(l, C_x) = \{l, b, r, U, V, W, M_x\}, \tag{A1}$$

where l and b are Galactic longitude and latitude, r is distance, U, V and W are the three components of a star's Galactic velocity, C_x represents various colours, and M_x absolute magnitudes in corresponding filters. The model values of distance and velocity are dependent on the Galactic longitude of a candidate star, while the model absolute magnitude is dependent on the star's colour. For the application to PMS stars in the Sco-Cen subgroups, we have used Siess isochrones (Siess et al. 2000) of 6 Myr for US and 16 Myr for UCL and LCC for the group models (M_g) and an older main-sequence isochrone for the field model (M_f).

For the kinematic models, we employ the same linear models in Galactic longitude for the group model, and the Galactic thin disk model of (Robin et al. 2003), as were used in Rizzuto et al. (2011).

We then calculate the model likelihood ratio for these two model for each stars according to equations 10 and 11 of (Rizzuto et al. 2011);

$$R = \frac{P(M_g|D)}{P(M_f|D)} = \frac{P(M_g)}{P(M_f)} \frac{\int P(D|\boldsymbol{\phi}_g, M_g) P(\boldsymbol{\phi}_g|M_g) \mathrm{d}\boldsymbol{\phi}_g}{\int P(D|\boldsymbol{\phi}_f, M_f) P(\boldsymbol{\phi}_f|M_f) \mathrm{d}\boldsymbol{\phi}_f}, \tag{A2}$$

where again, $M_{g,f}$ represents the association and field models, and $\phi_{g,f}$ represents the set of parameters, or a parameter vector derived from the models, which can be directly compared to the data D. The data are compiled from positions and proper motions taken from the UCAC4 catalog (Zacharias et al. 2013) and any available radial velocities in the RAVE catalog (Steinmetz et al. 2006),and a photometric distance calculated from the APASS B and V band photometry (Henden et al. 2012) and 2MASS J,H and K photometry (Skrutskie et al. 2006), using the model isochrones. Included in our distance estimate was a multiplicity photometric bias correction. This estimate was based on the expected multiplicity statistics of G, K and M-type stars, taken from Kraus et al. (2011), which indicates ∼50% of solar type stars have a companion. Combined with a standard initial mass function for the companion, this produces an average multiplicity bias of 0.2 magnitudes. Our photometric distances are thus calculated by adjusting the measured photometry by 0.2 magnitudes and then calculating a distance based on an interpolated isochrone magnitude. We define the uncertainty on the photometric distance conservatively to be 20%, or approximately ±0.4 magnitudes. This calculation is done for every star in our sample for both the association and field models.

With the inclusion of the photometric distances, we then calculate the model likelihood ratio integrals in the same way as described in Rizzuto et al. (2011) with a difference only present in how the distance and proper-motion integrals are treated. Equations A3, A4 and A5 show the details of the terms in the integrals of equation A2. For the high-mass stars, for which relatively well-defined parallax measurements were available, we treated the distance and parallel proper motion (proper motion in the direction of the association movement) integrals separately. For the larger distance and proper motion uncertainties of the low-mass stars, the two dimensional probability distribution in proper motion-parallax space is not symmetrical. This means that separating the proper motion and parallax integrals would inadequately describe the true value of the two dimensional integral. We address this issue by first sampling from the model distance distribution and then comparing the sampled values to the photometric distance measures and proper motion. We take 10^5 and 10^6 random samples of $(U, V, W, r)_{g,f}$ for the group and field models respectively to calculate the integrals. More samples are required for adequate sampling of the field model due to the larger spread of possible values. The key difference here when compared to the high-mass selection of Rizzuto et al. (2011) is that we also sample random distances from the distributions. The following equation describes the velocity distributions for both the field and the group models;

$$P(\boldsymbol{\phi}_{g,f}|M_{g,f}) \propto \exp\left(-\frac{(U - U_{g,f}(l))^2}{2\sigma^2_{U_{g,f}}}\right) + \left(-\frac{(V - V_{g,f}(l))^2}{2\sigma^2_{V_{g,f}}}\right) + \left(-\frac{(W - W_{g,f}(l))^2}{2\sigma^2_{W_{g,f}}}\right). \tag{A3}$$

where U, V, W and r represent the three components of the Galactic velocity and distance, with subscripts g and f indicating that the values are the corresponding expected values for the two models. The distance distribution for the group is also taken to be a normal distribution, as in Rizzuto et al. (2011);

$$\exp\left(-\frac{(r - r_{g,f}(l))^2}{2\sigma^2_{r_{g,f}}}\right) \tag{A4}$$

where r is the sampled distance and $r_{g,f}$ is the expected distance. Note that the model distribution means are a function of

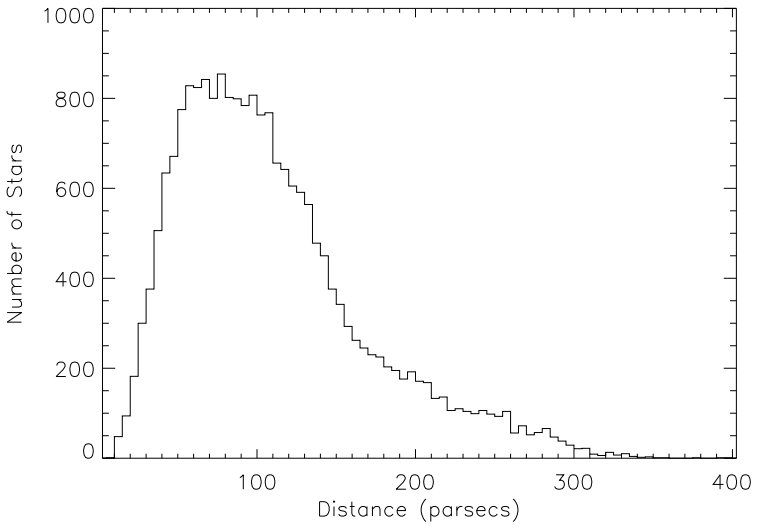

Figure A1. Field photometric distance distribution, showing features of the input catalog magnitude and colour cuts, and the isochrone used in estimation of the distances.

the Galactic longitude of the star being examined. For the field model, the distance distribution is not as directly describable as that of the group model. Instead, we construct the field distribution by taking all the calculated photometric distances for the field model and then take the samples from this using rejection sampling. Figure A1 shows the field distribution used in the sampling for the field model.

The final term in equation A2 is then given by;

$$P(D|\boldsymbol{\phi}_{g,f}) \propto \exp\left(-\frac{\mu_{\perp}^2}{2\sigma_{\mu_{\perp}}^2} - \frac{(\nu_r - \nu_{r_{g,f}})^2}{2\sigma_{\nu_r}^2} - \frac{(\mu_{\parallel} - \frac{\mu_{\parallel_{g,f}}}{r})^2}{2\sigma_{\mu_{\parallel}}^2} - \frac{(\pi_{g,f} - \frac{1}{r})^2}{2\sigma_{\pi_{g,f}}^2}\right), \tag{A5}$$

where $\mu_{\parallel}$ and $\mu_{\perp}$ are the star proper motions in the direction parallel to and perpendicular to the expected direction of motion for a given set of (U, V, W). For more information regarding this coordinate system, including procedures for transforming to and from equatorial coordinates, see de Zeeuw et al. (1999) and Rizzuto et al. (2011). $\pi_{g,f}$ is the calculated photometric parallax for the group and field models respectively, and ν_r is the radial velocity, which in the vast majority of cases is unconstrained and does not influence the integrals. With the model likelihood ratio we then determine the probability of membership, given by $R/(R+1)$.

Table 1. Summary of WiFeS observations of candidate Upper-Scorpius members; the V magnitude provided is either taken from APASS, where available, or interpolated from J and K according to the Kepler K2 instructions.

R.A. (J2000.0)	Decl. (J2000.0)	MJD	V (mag)	K (mag)	μ_α (mas)	μ_δ (mas)	Source	P_{mem}	T (sec)	SNR	M?
15 39 06.96	-26 46 32.1	56462	12.5	8.7	-35.3	-41.7	a	31	90	131	Y
15 37 42.74	-25 26 15.8	56462	13.5	9.7	-14.6	-26.7	a	85	90	80	
15 35 32.30	-25 37 14.1	56462	11.7	8.4	-9.0	-22.9	a	69	90	116	
15 41 31.21	-25 20 36.3	56462	10.0	7.2	-16.9	-28.7	a	86	90	151	Y
16 02 00.39	-22 21 23.9	56462	12.9	8.8	-16.6	-31.2	a	96	90	95	Y
16 02 08.45	-22 54 59.1	56462	13.6	9.6	-14.6	-22.8	a	97	120	93	Y
16 00 42.77	-21 27 38.0	56462	12.8	8.9	-11.5	-25.8	a	80	90	115	Y
16 00 40.56	-22 00 32.2	56462	11.2	8.4	-12.4	-20.4	a	89	90	140	Y
15 58 12.70	-23 28 36.4	56462	10.4	8.0	-11.1	-22.1	a	82	90	193	Y
15 59 59.95	-22 20 36.8	56462	12.9	8.6	-13.9	-24.1	a	96	90	107	Y
16 00 14.91	-21 01 31.7	56462	11.9	9.0	-14.3	-17.3	a	46	60	123	
16 00 13.30	-24 18 10.7	56462	13.6	9.5	-11.7	-23.8	a	94	90	91	Y
15 59 10.29	-26 46 50.0	56462	12.3	9.6	-6.6	-16.3	a	57	90	134	
15 49 21.00	-26 00 06.3	56462	11.2	7.9	-16.5	-26.4	a	89	90	139	Y
15 48 32.74	-28 44 15.6	56462	11.2	8.3	-7.5	-16.2	a	32	90	126	
15 53 47.13	-25 33 43.0	56462	11.5	8.6	-10.5	-21.7	a	77	90	101	
15 53 06.83	-22 47 17.4	56462	13.5	8.7	-14.0	-24.8	a	97	90	104	Y
15 55 02.14	-21 49 43.5	56462	12.4	8.6	-15.3	-22.4	a	90	90	112	Y
15 57 34.31	-23 21 12.3	56462	12.8	9.0	-15.3	-26.3	b		90	98	Y
15 57 16.74	-25 29 19.3	56462	12.5	8.9	-14.0	-20.0	a	80	90	85	Y
15 56 55.46	-22 58 40.4	56462	13.5	9.4	-12.8	-24.1	a	95	90	49	Y
15 56 06.96	-28 52 41.4	56462	10.1	7.4	-11.2	-18.5	a	75	90	142	
16 04 05.13	-27 35 23.0	56462	10.5	8.5	-26.6	-32.9	a	28	90	113	
16 09 30.31	-21 04 58.9	56462	12.8	8.9	-9.8	-21.0	a	88	90	124	Y
16 05 20.11	-22 56 04.7	56462	12.2	9.4	-9.0	-21.0	a	12	90	117	
16 05 21.57	-18 21 41.2	56462	12.2	8.1	-6.9	-19.6	a	79	90	100	Y
16 05 38.16	-20 39 47.0	56462	12.6	8.8	-8.8	-24.2	a	82	90	126	Y
16 06 43.86	-19 08 05.5	56462	13.1	9.2	-5.9	-21.3	a	85	90	112	Y
16 06 47.94	-18 41 43.8	56462	12.7	9.0	-6.2	-20.0	a	72	90	121	Y
16 08 01.42	-20 27 41.7	56462	13.5	9.3	-11.1	-20.5	b		90	33	Y
16 21 54.67	-20 43 09.1	56462	12.5	9.2	-18.2	-29.5	a	22	90	109	Y
16 07 40.06	-21 48 42.7	56462	13.5	9.7	-10.8	-17.8	a	88	90	79	Y
16 12 22.17	-27 12 52.5	56462	11.6	9.5	-12.9	-27.4	a	93	90	134	
16 12 06.68	-30 10 27.1	56462	13.3	9.3	-14.9	-20.6	a	73	90	99	Y
16 13 00.66	-26 58 02.2	56462	20.0	11.5	-6.0	-10.3	a	40	90	81	
16 14 38.77	-18 40 50.6	56462	12.9	9.6	-16.1	-16.2	a	46	90	97	
16 15 33.11	-27 07 58.8	56462	13.9	9.8	-12.0	-23.7	a	95	90	67	Y
16 15 35.86	-25 29 01.0	56462	12.4	8.7	-10.1	-24.0	a	80	90	102	Y
16 15 59.86	-23 25 04.5	56462	11.9	8.5	-6.6	-25.3	a	70	90	86	Y
16 16 51.30	-24 33 27.7	56462	9.7	7.7	-10.3	-18.2	a	78	90	96	Y
16 16 44.08	-23 55 45.7	56462	11.1	7.7	-17.9	-24.2	a	80	90	72	
16 17 31.38	-23 03 36.0	56462	10.1	8.0	-10.1	-16.6	a	53	90	112	Y
16 17 54.81	-24 43 33.7	56462	9.8	7.8	-8.5	-19.7	a	70	90	92	
16 18 19.98	-20 05 34.9	56462	10.4	7.9	-10.3	-25.0	a	83	90	91	Y
16 21 57.69	-24 29 43.5	56462	10.2	7.6	-10.6	-22.3	a	80	90	78	
15 33 17.26	-23 25 34.1	56756	12.1	8.6	-7.7	-22.2	a	59	90	70	
15 37 49.29	-20 29 18.3	56756	11.5	8.6	-16.5	-20.5	a	82	90	31	
15 40 27.32	-19 57 43.7	56756	10.4	7.4	-17.7	-17.6	a	72	90	25	
15 39 29.69	-23 11 19.9	56756	10.7	8.1	-16.3	-16.5	a	70	90	33	
15 42 26.21	-22 47 46.0	56756	13.0	8.6	-13.8	-20.9	a	97	90	38	Y
15 45 09.71	-25 12 43.0	56756	13.8	9.7	-15.6	-16.6	a	63	90	48	Y
15 47 10.63	-17 36 24.3	56756	13.9	9.6	-17.8	-24.1	a	86	90	26	Y
15 46 27.26	-25 18 46.8	56756	11.4	7.9	-18.4	-18.6	a	73	90	85	
15 47 43.31	-18 19 15.4	56756	13.7	9.8	-11.5	-21.8	a	92	90	56	Y
15 49 25.09	-28 43 52.8	56756	13.9	9.7	-19.2	-25.4	a	95	90	34	Y
15 54 03.57	-29 20 15.6	56756	12.5	8.7	-17.5	-18.8	a	75	90	79	Y

Continued on next page

Table 1. Summary of WiFeS observations of candidate Upper-Scorpius members; the V magnitude provided is either taken from APASS, where available, or interpolated from J and K according to the Kepler K2 instructions.

R.A. (J2000.0)	Decl. (J2000.0)	MJD	V (mag)	K (mag)	μ_α (mas)	μ_δ (mas)	Source	P_{mem}	T (sec)	SNR	M?
15 50 49.08	-16 34 48.3	56756	12.0	9.1	-13.8	-17.4	a	56	90	71	
15 51 50.27	-22 38 18.8	56756	11.5	8.2	-14.0	-15.7	a	67	90	69	
16 21 54.67	-20 43 09.1	56756	12.5	9.2	-18.2	-29.5	a	22	90	86	Y
15 56 47.69	-19 50 07.6	56756	12.8	8.9	-11.3	-20.9	a	94	90	80	Y
16 01 32.73	-22 19 37.8	56756	11.1	8.2	-7.5	-13.9	a	39	90	59	
16 02 31.96	-28 13 45.2	56756	10.6	7.7	-24.7	-30.6	a	72	90	70	
16 02 24.61	-22 00 24.8	56756	13.3	9.4	-12.8	-24.1	a	91	90	35	Y
16 16 02.92	-24 30 54.8	56756	13.7	9.0	-10.2	-22.7	a	95	90	25	Y
16 16 17.20	-26 09 10.2	56756	13.1	8.7	-8.7	-25.5	a	92	90	28	Y
16 16 46.63	-34 14 14.4	56756	11.3	8.4	-19.1	-29.6	a	74	90	65	
16 17 22.98	-21 21 11.9	56756	13.4	9.3	-7.5	-20.1	a	83	90	51	Y
16 19 14.74	-25 32 31.3	56756	12.9	8.7	-5.6	-20.8	a	73	90	58	Y
16 19 31.39	-25 18 12.8	56756	13.2	8.9	-7.6	-20.5	a	86	90	46	Y
16 19 45.38	-21 47 57.8	56756	12.8	9.1	-12.8	-22.4	a	93	90	39	Y
16 20 27.24	-21 26 06.9	56756	13.1	9.2	-9.0	-21.4	a	94	90	29	Y
16 20 45.08	-14 49 58.0	56756	13.6	9.3	-7.3	-13.5	a	82	90	30	
16 20 45.79	-28 49 20.1	56756	13.7	9.1	-12.9	-24.0	a	92	90	21	Y
16 23 18.69	-26 23 43.3	56824	12.4	7.0	-14.3	-19.2	b		60	29	
16 23 22.93	-26 22 16.1	56824	9.6	7.9	-20.4	-31.9	b		60	36	Y
16 24 49.82	-26 23 45.9	56824	11.8	7.3	-15.2	-18.9	b		60	23	
16 25 35.72	-26 09 33.8	56824	10.0	6.8	-12.0	-13.4	b		60	49	
16 25 57.91	-26 00 37.3	56824	12.9	8.5	-7.9	-19.9	a	81	90	26	Y
16 25 56.96	-26 00 40.6	56824	13.4	9.3	-1.1	-9.5	a	6	90	26	
16 25 57.91	-26 00 37.3	56824	12.9	8.5	-7.9	-19.9	a	81	90	90	Y
16 28 52.01	-26 11 55.4	56824	9.5	8.2	-16.3	-28.5	b		60	31	
16 12 36.05	-27 23 03.2	56824	11.2	7.2	-9.9	-13.1	b		90	54	Y
16 12 46.71	-27 33 28.7	56824	10.5	7.1	-10.6	-17.2	b		90	30	
16 15 25.71	-28 27 53.1	56824	11.4	6.9	-10.5	-13.0	b		90	114	
16 18 32.97	-27 57 29.1	56824	10.8	7.0	-1.7	-23.3	a	17	90	33	
16 16 09.07	-27 56 23.3	56824	11.2	7.9	-7.7	-11.9	a	11	90	17	
16 13 28.04	-27 24 13.4	56824	8.6	7.5	-11.9	-26.1	b		90	30	
16 13 47.82	-27 47 34.0	56824	9.3	8.0	-8.4	-22.7	b		90	113	
16 21 54.67	-20 43 09.1	56824	12.5	9.2	-18.2	-29.5	a	22	90	34	Y
16 34 22.40	-21 54 31.0	56824	13.6	9.1	-6.3	-17.0	a	85	90	16	
16 25 16.90	-23 22 03.6	56824	14.3	9.0	-6.3	-36.5	a	61	90	46	Y
16 11 04.80	-23 33 16.6	56824	13.3	9.7	-6.8	-16.5	a	78	90	35	Y
16 08 04.11	-26 40 44.9	56824	12.8	9.1	-9.9	-22.2	b		90	24	Y
16 08 56.96	-28 35 57.4	56824	13.4	9.6	-6.4	-20.6	a	92	90	32	Y
15 59 52.69	-25 26 29.2	56824	13.5	9.7	-19.8	-26.6	a	93	90	45	Y
16 15 19.49	-25 40 12.0	56824	13.2	9.1	-9.4	-23.6	a	94	90	52	Y
16 14 07.35	-22 17 32.2	56824	13.3	9.1	-9.3	-22.0	a	95	90	39	Y
16 14 42.70	-25 12 09.7	56824	14.5	9.3	-13.8	-18.7	a	91	90	35	
16 24 19.21	-19 19 17.4	56824	14.0	9.4	-19.7	-27.2	a	85	90	58	
16 24 09.43	-21 34 07.3	56824	15.0	10.5	-2.8	-28.8	a	89	90	14	Y
16 03 46.95	-22 45 24.7	56824	13.2	9.1	-12.6	-26.0	b		90	36	Y
15 59 44.27	-20 29 23.4	56824	15.3	10.4	-5.2	-30.6	a	88	90	10	Y
16 33 58.75	-27 42 16.7	56824	14.1	9.3	-10.2	-24.1	a	92	90	36	
16 12 05.05	-20 43 40.5	56824	13.5	9.1	-10.3	-22.7	a	95	90	45	Y
16 12 35.32	-20 34 34.0	56824	13.5	9.3	-17.2	-32.7	b		90	49	Y
16 11 26.03	-26 31 55.9	56824	13.7	9.6	-9.4	-25.5	a	96	90	36	Y
16 09 39.70	-22 00 46.6	56824	13.5	9.3	-10.1	-20.3	a	92	90	43	Y
16 30 01.36	-15 43 11.1	56824	13.5	9.5	-10.3	-13.3	b		90	34	
16 28 23.58	-27 22 41.3	56824	14.2	9.3	-4.8	-13.4	a	35	90	44	
16 03 01.77	-26 26 21.9	56824	13.5	9.7	-12.2	-22.5	a	98	90	39	Y
16 14 02.27	-18 52 43.9	56824	14.5	9.0	-7.5	-13.4	b		90	28	
16 15 00.60	-29 19 34.9	56824	13.2	9.4	-13.3	-23.4	a	96	90	47	Y

Continued on next page

Table 1. Summary of WiFeS observations of candidate Upper-Scorpius members; the V magnitude provided is either taken from APASS, where available, or interpolated from J and K according to the Kepler K2 instructions.

R.A. (J2000.0)	Decl. (J2000.0)	MJD	V (mag)	K (mag)	μ_α (mas)	μ_δ (mas)	Source	P_{mem}	T (sec)	SNR	M?
16 15 12.40	-23 18 45.3	56824	13.7	9.7	-7.8	-25.5	a	74	90	28	Y
16 09 31.66	-22 29 22.4	56824	13.3	9.2	-8.8	-18.9	a	92	90	53	Y
16 22 08.59	-29 15 06.4	56824	13.3	9.7	-11.9	-27.7	a	90	90	53	Y
16 30 29.35	-16 01 52.9	56824	13.3	9.9	-1.8	-17.5	b		90	34	
16 25 35.04	-23 32 55.0	56824	14.2	8.9	-5.4	-26.3	b		90	42	Y
16 34 17.86	-28 59 37.4	56824	13.9	9.2	2.0	-22.6	b		90	29	
16 29 35.57	-25 04 23.9	56824	13.7	9.3	-15.5	-23.7	b		90	16	
16 10 28.23	-27 56 39.5	56824	13.1	9.6	-6.4	-36.4	b		90	37	
16 23 22.08	-21 25 49.0	56825	14.1	9.7	-6.0	-22.3	a	92	90	20	
16 26 19.98	-22 33 02.5	56825	14.1	9.8	-16.0	-20.6	a	95	90	41	Y
16 27 27.66	-28 21 50.4	56825	13.5	10.0	-9.6	-27.8	a	93	90	48	Y
16 25 49.24	-25 54 37.3	56825	14.4	9.5	-12.0	-24.4	a	93	90	74	Y
16 25 28.81	-26 07 53.8	56825	14.3	9.9	-9.9	-25.8	a	97	90	57	Y
16 22 20.42	-28 37 16.4	56825	13.8	9.8	-16.4	-32.2	a	81	90	68	
16 25 02.37	-23 21 45.1	56825	14.6	9.3	-4.6	-30.4	a	72	90	59	Y
16 00 49.73	-23 38 43.2	56825	13.7	9.7	-14.8	-27.3	b		90	66	Y
16 01 22.34	-19 37 22.3	56825	13.9	9.6	-10.1	-17.6	b		90	67	Y
16 20 21.64	-20 05 34.8	56825	15.4	11.0	-14.6	-14.4	b		90	6	Y
16 08 56.29	-21 48 48.9	56825	13.5	9.6	-10.2	-22.6	b		90	69	Y
16 04 06.71	-26 37 07.1	56825	13.9	10.0	-10.3	-32.2	a	95	90	53	Y
16 32 54.35	-19 29 46.9	56825	14.5	9.7	1.6	-17.5	a	23	90	63	
16 02 58.44	-25 45 29.9	56825	13.8	10.2	-20.0	-33.6	a	73	90	41	
16 21 54.67	-20 43 09.1	56825	12.5	9.2	-18.2	-29.5	a	22	90	150	Y
16 30 01.50	-28 15 29.5	56825	14.5	9.8	-8.0	-14.6	a	68	90	58	
16 24 15.52	-25 44 34.5	56825	14.3	9.6	-13.0	-20.3	b		90	67	Y
16 19 34.35	-20 13 50.2	56825	14.2	9.8	-0.8	-37.3	a	2	90	65	
16 17 30.32	-24 38 39.2	56825	14.5	9.7	-10.1	-22.3	a	94	90	45	Y
16 20 50.95	-22 53 40.1	56825	14.5	9.8	-13.1	-21.7	a	95	120	55	Y
16 15 11.05	-23 22 42.7	56825	13.8	9.8	-9.1	-24.1	a	68	90	66	Y
16 14 41.26	-25 56 05.3	56825	14.3	10.1	-11.4	-22.9	a	97	120	60	Y
16 07 51.37	-17 18 23.2	56825	13.9	10.0	-5.7	-18.0	a	93	120	54	Y
15 56 12.17	-23 54 07.7	56825	13.9	10.2	-20.5	-32.9	a	85	120	26	Y
16 18 41.89	-18 32 39.8	56825	13.9	10.1	-20.4	-27.0	a	92	120	41	
15 59 38.07	-26 03 23.5	56825	13.8	10.3	-11.3	-29.0	a	92	120	27	Y
16 16 33.45	-25 52 36.8	56825	14.1	9.6	-8.7	-21.2	a	93	90	57	Y
16 14 52.70	-23 08 02.7	56825	13.6	9.6	-10.4	-19.5	a	96	90	51	Y
16 33 34.97	-18 32 53.9	56825	14.1	10.4	-13.4	-23.0	a	96	90	29	Y
16 18 42.10	-18 33 29.0	56825	13.7	9.9	-16.8	-26.4	a	96	90	63	
16 34 38.27	-28 35 50.5	56825	13.8	9.8	-10.1	-23.8	a	97	90	62	Y
16 23 57.91	-26 02 29.9	56825	14.0	10.0	-9.3	-19.7	a	96	90	75	Y
16 23 04.74	-27 59 25.4	56825	13.5	9.6	-10.2	-22.6	a	83	90	83	Y
16 22 44.07	-21 42 22.2	56825	14.2	9.9	-11.5	-19.3	a	95	90	40	Y
15 56 25.11	-20 16 15.8	56825	13.8	9.9	-13.4	-22.5	a	97	120	33	Y
16 35 21.67	-15 38 19.9	56825	14.2	9.7	-7.5	-14.0	b		90	77	
16 14 10.12	-22 17 23.5	56825	13.9	9.8	-5.2	-17.8	a	85	90	42	Y
16 23 37.53	-25 35 34.1	56825	14.3	9.5	-2.6	-16.2	b		90	71	
16 22 20.93	-27 47 09.6	56825	13.3	9.5	-7.1	-28.2	a	91	120	72	Y
16 17 55.02	-27 11 30.4	56825	13.5	9.9	-5.9	-23.7	a	88	90	64	Y
16 14 12.58	-24 54 28.8	56825	13.8	9.9	-7.7	-19.4	a	56	90	65	Y
16 26 28.04	-25 26 47.8	56825	14.5	9.1	-6.1	-30.2	b		90	76	Y
16 13 36.44	-23 26 27.0	56825	13.5	9.3	-4.2	-20.6	a	86	90	67	Y
16 20 36.41	-21 23 12.0	56825	13.8	10.0	-10.8	-22.1	a	97	120	39	Y
16 12 13.69	-24 31 36.9	56825	14.2	10.1	-16.4	-21.9	a	97	120	52	Y
16 10 26.25	-22 09 10.5	56825	13.6	9.0	-8.9	-24.1	b		90	66	Y
16 15 47.77	-25 03 29.7	56825	13.7	10.3	-15.3	-35.6	a	9	120	48	
16 28 45.15	-27 12 19.3	56825	14.4	9.8	-10.5	-23.8	a	96	120	56	

Continued on next page

Table 1. Summary of WiFeS observations of candidate Upper-Scorpius members; the V magnitude provided is either taken from APASS, where available, or interpolated from J and K according to the Kepler K2 instructions.

R.A. (J2000.0)	Decl. (J2000.0)	MJD	V (mag)	K (mag)	μ_α (mas)	μ_δ (mas)	Source	P_{mem}	T (sec)	SNR	M?
16 09 29.70	-22 00 58.0	56825	13.9	9.6	-16.9	-19.2	b		120	77	Y
16 11 05.67	-21 44 03.3	56825	13.6	9.2	-9.6	-23.3	b		120	77	Y
16 35 42.10	-23 10 04.0	56825	14.6	9.9	-1.2	-18.1	a	58	120	65	
16 35 23.82	-22 29 54.7	56825	14.8	9.6	-8.2	-13.1	a	44	120	78	
16 14 27.55	-27 09 16.7	56825	14.3	9.5	-8.9	-15.0	b		120	83	
16 10 02.31	-24 34 18.6	56826	13.8	10.4	-12.8	-37.1	a	1	120	68	
16 21 18.30	-19 45 18.5	56826	13.9	10.3	-17.2	-27.2	a	84	120	48	
16 22 51.59	-27 55 37.3	56826	13.9	10.2	-11.9	-27.9	a	97	120	63	
16 23 59.02	-27 36 03.7	56826	13.1	9.4	-3.7	-21.6	a	20	120	82	Y
15 55 41.41	-20 43 15.1	56826	13.9	9.4	-14.3	-21.8	b		120	89	Y
16 23 37.94	-24 36 30.4	56826	14.1	9.9	-6.2	-12.6	a	8	120	90	
15 58 06.94	-26 23 46.7	56826	14.0	10.2	-10.9	-27.2	a	97	120	82	Y
16 17 16.50	-23 27 57.1	56826	14.4	10.2	-12.5	-26.6	b		120	64	Y
16 24 11.77	-19 55 58.3	56826	14.6	9.9	-10.8	-18.3	a	92	480	82	Y
16 15 27.51	-26 27 28.1	56826	15.5	11.2	-11.3	-25.0	b		300	36	Y
16 17 29.95	-24 51 03.2	56826	14.7	9.8	-9.0	-21.3	a	92	300	68	Y
16 20 53.01	-20 19 20.3	56826	14.6	10.0	-10.0	-18.6	a	93	300	78	
16 22 54.78	-21 38 09.3	56826	14.2	10.1	-10.0	-24.5	a	97	300	84	Y
16 21 48.54	-25 17 26.6	56826	14.6	10.0	-10.4	-19.8	a	94	300	99	Y
16 20 32.46	-22 57 45.4	56826	14.8	9.8	-7.4	-22.2	a	89	300	76	Y
15 57 00.93	-20 24 48.2	56826	14.0	10.3	-14.0	-21.5	a	97	300	76	
16 07 30.38	-25 46 27.0	56826	14.1	10.1	-9.7	-23.9	a	97	300	82	Y
16 09 49.55	-24 44 46.8	56826	14.0	10.1	-16.0	-21.9	b		300	66	Y
16 22 05.88	-21 21 55.6	56826	14.0	10.0	-11.7	-26.1	a	79	300	112	Y
16 27 33.22	-28 21 09.8	56826	14.0	10.5	-12.6	-25.1	a	87	300	71	Y
15 57 03.69	-23 04 48.3	56826	14.0	10.2	-10.6	-19.4	a	95	300	70	Y
15 57 23.92	-20 51 45.4	56826	14.1	9.8	-7.0	-19.1	b		300	72	Y
16 03 38.30	-18 54 07.7	56826	14.1	9.5	-7.8	-20.8	a	94	300	79	Y
16 02 35.89	-23 20 17.1	56826	14.1	10.2	-7.1	-20.4	a	94	300	61	Y
15 56 20.60	-23 36 10.0	56826	14.2	10.3	-9.2	-16.6	b		300	71	Y
16 00 00.37	-22 32 59.5	56826	14.2	9.8	-12.8	-21.3	a	96	300	90	
16 14 49.89	-21 39 32.2	56826	14.1	10.1	-7.7	-23.7	a	33	300	74	Y
16 19 02.15	-21 38 09.7	56826	14.1	10.4	-8.2	-23.3	a	96	300	65	Y
16 14 03.80	-24 53 08.9	56826	14.1	10.0	-9.4	-18.3	a	27	300	56	Y
16 08 40.25	-27 33 39.7	56826	14.1	10.6	-17.8	-28.1	a	67	300	70	
16 09 35.76	-21 38 05.8	56826	14.2	9.9	-12.7	-20.5	a	95	300	81	Y
15 55 05.13	-20 26 07.7	56826	14.2	9.7	-12.0	-24.6	b		300	76	Y
15 56 24.92	-25 41 20.3	56826	14.2	10.4	-15.7	-23.0	b		300	71	Y
15 59 18.72	-26 48 14.1	56826	14.2	10.7	-17.6	-33.6	a	46	300	70	
15 55 08.53	-23 18 51.1	56826	14.2	9.9	-13.6	-21.1	b		300	87	Y
16 09 31.10	-20 41 46.0	56826	14.3	10.1	-14.4	-25.2	a	98	300	49	Y
16 19 48.36	-22 12 51.8	56826	14.2	10.3	-14.5	-22.7	a	97	300	49	Y
16 22 43.55	-18 52 35.8	56826	14.2	10.6	-11.6	-21.8	a	93	300	63	
16 22 06.59	-21 27 08.9	56826	14.2	10.1	-11.1	-30.2	a	96	300	68	Y
16 23 57.23	-26 20 24.6	56826	14.2	10.2	-8.3	-23.0	a	97	300	63	Y
16 25 23.27	-27 27 31.5	56826	14.2	10.7	-13.8	-25.2	a	11	300	48	Y
16 26 54.09	-27 35 07.7	56826	14.2	10.7	-6.5	-24.1	a	61	300	58	
16 19 16.09	-29 15 12.7	56826	14.1	10.4	-12.7	-25.2	a	95	300	66	Y
16 34 58.06	-22 57 20.5	56826	14.2	10.4	-8.6	-25.4	a	96	300	42	
16 21 55.94	-27 05 03.4	56826	14.2	10.8	-19.1	-25.9	a	27	300	39	Y
16 01 13.99	-25 16 28.2	56826	14.3	10.4	-14.3	-19.9	b		300	37	Y
16 19 48.78	-22 24 47.5	56826	14.3	10.8	-32.9	-36.4	a	7	300	28	Y
16 13 56.62	-24 57 56.8	56826	14.3	10.2	-9.4	-24.2	a	97	300	63	Y
16 11 17.45	-24 41 20.4	56826	14.3	10.4	-7.2	-27.2	a	94	300	62	Y
16 26 34.95	-25 11 40.9	56826	14.3	10.0	-6.4	-27.2	b		300	101	Y
16 01 08.97	-26 45 10.6	56826	14.3	10.6	-15.2	-23.8	a	85	300	26	Y

Continued on next page

Table 1. Summary of WiFeS observations of candidate Upper-Scorpius members; the V magnitude provided is either taken from APASS, where available, or interpolated from J and K according to the Kepler K2 instructions.

R.A. (J2000.0)	Decl. (J2000.0)	MJD	V (mag)	K (mag)	μ_α (mas)	μ_δ (mas)	Source	P_{mem}	T (sec)	SNR	M?
16 21 29.55	-25 29 43.1	56826	14.3	10.2	-0.8	-24.1	a	72	300	71	Y
16 15 36.43	-26 22 09.2	56826	14.3	10.2	-3.4	-24.7	a	88	300	35	Y
16 10 14.46	-19 51 37.5	56826	14.3	10.2	-5.8	-24.0	a	78	300	56	Y
16 13 09.79	-20 44 59.1	56826	14.3	9.9	-10.3	-19.0	b		300	64	Y
16 13 21.91	-21 36 13.7	56826	14.3	10.0	-6.5	-22.0	a	93	300	38	Y
16 00 12.17	-21 57 03.3	56826	14.3	10.3	-12.7	-24.0	b		300	36	Y
15 55 39.28	-20 53 07.3	56826	14.4	10.6	-9.8	-23.7	a	94	300	34	Y
16 13 32.79	-20 44 41.4	56826	14.4	10.1	-12.4	-24.0	b		300	68	Y
16 13 44.90	-24 34 14.4	56826	14.4	10.3	-11.7	-20.5	b		300	62	Y
16 17 26.15	-24 50 59.2	56826	14.4	9.9	-11.4	-14.6	a	82	300	62	Y
16 19 47.12	-22 03 11.2	56826	14.4	10.6	-6.3	-22.0	a	94	300	35	Y
15 57 42.47	-25 51 35.6	56826	14.4	10.8	-4.4	-29.2	a	27	300	28	Y
15 57 24.55	-20 38 38.2	56826	14.4	10.0	-12.2	-25.1	b		300	34	Y
16 31 05.80	-27 25 46.1	56826	14.3	10.5	-7.1	-20.7	a	95	300	41	Y
16 31 56.69	-28 46 12.7	56826	14.3	10.5	-14.3	-20.0	a	94	300	42	Y
16 29 56.63	-26 59 18.4	56826	14.3	10.4	-14.3	-25.8	a	97	300	48	Y
16 27 13.23	-20 04 25.7	56826	14.4	11.1	-19.9	-27.1	b		300	45	
16 21 15.84	-22 40 04.5	56826	14.5	9.8	-8.0	-18.6	a	92	300	37	Y
16 23 45.33	-29 08 04.5	56827	9.8	6.1	-11.7	-14.0	b		180	107	
16 22 43.79	-29 11 37.7	56827	11.4	8.0	-7.9	-13.9	a	25	180	115	
16 21 55.07	-21 52 04.3	56827	14.4	10.4	-9.4	-12.7	a	86	300	11	
16 23 41.97	-29 02 22.9	56827	12.0	7.1	-3.3	-18.2	b		180	112	
16 23 52.29	-27 59 13.6	56827	11.3	7.8	-16.9	-21.8	a	78	180	91	
16 24 18.59	-28 42 54.1	56827	10.5	8.1	-14.8	-25.7	a	77	180	25	
16 24 18.60	-28 54 47.5	56827	11.2	8.3	-4.6	-15.8	a	27	180	62	Y
16 26 23.43	-27 39 00.5	56827	10.7	8.1	-14.1	-25.6	a	72	180	27	
16 30 39.35	-27 15 10.4	56827	10.4	7.5	-4.6	-14.4	a	16	180	53	
16 31 55.53	-29 02 14.3	56827	11.2	8.0	-6.6	-13.4	a	15	180	79	
16 00 52.72	-25 23 42.7	56827	14.4	10.4	-13.9	-17.8	a	85	300	21	Y
16 30 07.45	-17 34 35.8	56827	14.4	10.9	-19.2	-24.5	a	1	300	6	
16 23 32.34	-25 23 48.5	56827	11.4	7.7	-7.3	-23.7	a	76	180	94	Y
16 26 19.32	-23 43 20.5	56827	20.0	9.0	19.9	-34.7	a	0	180	100	
16 03 37.77	-18 45 08.3	56827	14.5	9.8	-7.8	-21.4	b		300	28	Y
16 21 15.84	-22 40 04.5	56827	14.5	9.8	-8.0	-18.6	a	92	300	51	Y
16 12 08.14	-25 47 57.9	56827	14.4	10.3	-14.1	-23.6	a	98	300	44	Y
16 26 32.77	-26 22 59.0	56827	14.4	10.5	-8.7	-30.1	b		300	13	Y
16 03 25.98	-26 27 32.2	56827	14.5	10.8	-17.8	-28.8	a	79	300	24	Y
16 13 38.40	-24 43 31.2	56827	14.5	10.4	-12.4	-22.2	a	97	300	58	Y
16 16 59.84	-21 54 27.3	56827	14.5	10.6	-8.9	-26.2	a	93	300	55	Y
16 03 34.94	-22 31 54.6	56827	14.5	10.9	-19.6	-30.3	a	39	300	35	
15 58 18.85	-19 15 44.9	56827	14.5	10.1	-12.5	-18.6	b		300	70	Y
16 19 52.87	-22 02 58.5	56827	14.5	11.1	-18.9	-32.3	b		300	41	
16 12 33.54	-25 43 27.6	56827	14.5	10.1	2.4	-9.7	a	37	300	22	Y
16 22 08.94	-21 40 37.2	56827	14.5	10.6	-15.7	-14.4	a	87	300	47	Y
15 59 08.65	-26 00 54.4	56827	14.5	10.8	-16.8	-20.2	a	90	300	29	Y
16 25 10.73	-26 09 55.2	56827	14.5	10.7	-17.8	-25.4	b		300	49	
16 23 10.10	-23 05 14.2	56827	14.5	10.2	-12.5	-6.3	a	9	300	57	
16 00 07.05	-23 40 48.7	56827	14.5	10.6	-11.5	-31.0	b		300	36	Y
16 27 09.51	-26 18 54.9	56827	14.5	10.8	-13.3	-24.9	b		300	36	Y
16 16 09.48	-22 43 43.8	56827	14.5	10.5	-4.8	-17.9	a	89	300	67	Y
16 13 06.28	-26 06 10.7	56827	14.5	10.9	-10.5	-20.7	a	85	300	36	Y
16 01 09.25	-19 07 59.1	56829	13.5	8.9	-2.9	-15.2	b		300	124	
15 55 29.81	-25 44 50.0	56829	13.5	9.1	-13.9	-27.2	b		300	98	Y
15 56 33.98	-25 30 08.4	56829	13.7	10.1	-19.3	-35.2	a	58	300	73	
15 58 58.21	-23 04 35.2	56829	13.8	9.9	-13.2	-23.3	a	96	180	40	Y
15 56 25.26	-26 28 28.6	56829	14.0	10.3	-18.2	-35.2	a	84	300	57	

Continued on next page

Table 1. Summary of WiFeS observations of candidate Upper-Scorpius members; the V magnitude provided is either taken from APASS, where available, or interpolated from J and K according to the Kepler K2 instructions.

R.A. (J2000.0)	Decl. (J2000.0)	MJD	V (mag)	K (mag)	μ_α (mas)	μ_δ (mas)	Source	P_{mem}	T (sec)	SNR	M?
16 00 49.89	-19 28 00.4	56829	13.7	9.7	-8.1	-21.2	b		180	30	Y
16 04 18.93	-24 30 39.3	56829	13.8	8.9	-9.3	-21.7	b		180	97	Y
16 10 05.02	-21 32 31.9	56829	13.9	8.9	-12.3	-22.6	a	91	180	72	Y
16 09 20.63	-22 22 05.7	56829	13.7	9.5	-9.5	-22.4	b		180	30	Y
16 16 01.52	-17 28 08.0	56829	13.6	11.1	-13.7	-11.7	b		300	60	
16 16 18.94	-25 42 28.7	56829	13.7	8.7	-9.4	-32.6	b		180	54	Y
16 26 19.64	-21 37 20.8	56829	13.7	9.4	-8.7	-24.2	a	94	180	89	Y
16 23 24.54	-17 17 27.1	56829	13.5	9.7	-12.1	-23.3	a	95	180	71	Y
16 12 47.66	-16 09 18.2	56829	13.8	10.0	-1.6	-18.2	b		180	34	
16 27 57.93	-25 24 18.8	56829	13.8	10.1	-9.6	-24.9	a	50	180	64	Y
16 35 06.26	-20 25 28.3	56829	13.8	9.6	-4.3	-27.5	a	87	180	58	Y
16 30 02.76	-27 27 00.5	56829	13.5	9.8	-10.3	-18.5	a	95	180	29	Y
16 25 55.41	-27 21 24.3	56829	13.5	10.0	-12.6	-23.2	a	94	180	47	Y
16 26 41.21	-22 00 09.5	56829	13.9	9.3	-19.9	-21.4	a	85	180	78	Y
16 33 38.83	-21 50 26.3	56829	13.9	8.9	-4.2	-16.4	a	44	180	96	Y
16 31 32.62	-27 19 46.1	56829	13.9	9.5	-5.8	-4.7	a	0	180	88	
16 21 41.26	-22 12 05.5	56829	13.9	9.9	-10.3	-20.2	a	97	180	46	Y
16 13 20.55	-22 29 15.9	56829	14.0	10.2	-9.2	-19.4	a	25	180	78	Y
16 12 39.94	-25 39 54.2	56829	14.0	10.4	-15.1	-28.0	a	94	180	45	
16 20 24.98	-21 50 23.9	56829	14.0	9.9	-14.3	-20.8	a	94	180	84	Y
15 58 28.56	-23 34 19.1	56829	14.5	10.4	-12.5	-27.5	a	97	300	66	Y
15 55 50.98	-25 19 39.4	56829	14.5	10.7	-15.3	-27.2	b		300	58	Y
16 35 11.02	-17 12 08.9	56829	14.5	10.2	-10.4	-13.4	b		300	107	
16 31 15.42	-26 57 15.1	56829	14.5	10.3	-10.8	-20.1	a	96	300	83	Y
16 08 16.95	-25 42 47.3	56829	14.5	11.0	-13.1	-21.3	a	47	300	39	
16 03 39.22	-18 51 29.3	56829	14.5	10.2	-9.6	-20.5	a	96	300	59	Y
16 01 59.88	-18 43 45.7	56829	14.6	10.2	-14.3	-21.9	b		300	71	Y
16 00 43.10	-24 30 50.5	56829	14.6	10.8	-10.6	-24.6	a	91	300	36	Y
16 11 32.87	-25 17 20.4	56829	14.6	10.8	-5.8	-21.6	a	85	360	40	
16 14 33.64	-20 04 29.9	56829	14.6	10.1	-3.1	-22.1	a	82	360	87	Y
16 03 51.75	-21 40 15.5	56829	14.6	10.6	-10.4	-20.6	b		360	39	Y
16 34 35.14	-26 58 03.1	56829	14.6	10.5	-6.5	-21.1	a	89	300	44	Y
16 20 06.16	-22 12 38.5	56829	14.6	10.7	-12.8	-24.9	a	96	360	71	Y
16 16 00.81	-22 14 19.3	56829	14.6	11.0	-7.1	-28.1	b		360	41	Y
15 56 42.45	-20 39 34.2	56829	14.6	10.3	-13.5	-27.7	a	98	360	77	Y
16 17 27.70	-24 21 02.6	56829	14.6	10.3	-2.9	-23.1	a	89	360	38	Y
16 19 48.86	-21 40 36.0	56829	14.6	10.8	-7.7	-19.7	a	94	360	58	Y
16 27 12.74	-25 04 01.8	56829	14.7	9.4	-3.4	-27.0	b		360	100	Y
16 27 40.92	-26 10 56.8	56829	14.7	10.5	-5.2	-20.9	a	93	360	58	
16 17 21.63	-23 25 00.4	56829	14.7	10.8	-5.3	-20.5	a	91	360	52	Y
16 23 17.41	-21 59 07.0	56829	14.7	10.2	-15.0	-23.8	a	96	360	51	Y
16 17 13.80	-22 51 58.5	56829	14.7	10.9	-9.3	-25.7	a	85	360	49	Y
16 03 14.91	-22 34 45.5	56829	14.7	10.7	-8.8	-26.3	b		360	30	Y
15 58 06.40	-23 40 41.9	56829	14.7	10.7	-11.3	-32.8	a	91	360	54	Y
16 12 50.83	-18 36 59.5	56829	14.7	9.6	-8.4	-15.6	b		360	67	
16 08 20.77	-21 31 23.4	56830	14.6	10.8	-14.2	-28.4	a	80	360	44	Y
15 59 01.93	-26 16 33.0	56830	14.6	11.3	-17.7	-27.9	b		360	26	Y
16 16 47.94	-24 40 28.2	56830	14.7	10.3	-7.8	-18.2	a	92	360	53	
15 58 36.20	-19 46 13.5	56830	14.8	10.7	-16.4	-19.5	a	95	360	52	Y
15 58 15.73	-20 21 36.8	56830	14.8	11.1	-4.5	-30.6	a	59	360	29	Y
15 56 34.26	-20 03 33.3	56830	14.8	10.9	-7.1	-17.1	b		360	35	Y
15 55 44.48	-22 06 42.7	56830	14.9	10.7	-17.6	-23.3	b		360	49	
16 01 34.47	-20 38 01.6	56830	14.9	11.3	-14.1	-22.5	b		360	40	
16 01 29.03	-25 09 06.9	56830	14.9	10.1	-10.7	-26.9	b		360	50	Y
16 07 14.02	-17 02 42.7	56830	14.9	10.8	-10.3	-20.5	a	97	360	57	Y
16 02 23.57	-22 59 33.3	56830	14.9	11.0	-8.4	-28.9	b		300	22	Y

Continued on next page

Table 1. Summary of WiFeS observations of candidate Upper-Scorpius members; the V magnitude provided is either taken from APASS, where available, or interpolated from J and K according to the Kepler K2 instructions.

R.A. (J2000.0)	Decl. (J2000.0)	MJD	V (mag)	K (mag)	μ_α (mas)	μ_δ (mas)	Source	P_{mem}	T (sec)	SNR	M?
16 14 52.41	-25 13 52.4	56830	14.9	10.5	-15.6	-21.9	a	97	360	43	Y
16 11 16.87	-26 39 33.1	56830	14.8	11.4	-8.4	-30.8	b		360	31	Y
16 09 07.78	-27 34 22.1	56830	14.8	11.4	-18.4	-35.0	b		360	36	
16 10 03.94	-27 28 48.0	56830	14.8	11.2	-17.7	-20.3	b		360	38	Y
16 09 52.88	-24 41 53.6	56830	14.8	10.9	-17.7	-24.3	b		360	33	Y
16 16 08.55	-20 41 51.5	56830	14.8	10.7	-11.2	-27.7	a	96	360	59	Y
16 12 17.24	-28 39 08.6	56830	14.8	11.3	0.3	-37.8	a	0	360	29	Y
16 31 43.62	-28 46 35.2	56830	14.8	11.0	-4.0	-18.8	b		360	28	
16 20 06.86	-22 47 32.1	56830	14.8	10.8	-4.6	-16.2	b		360	44	Y
16 26 20.16	-22 33 12.7	56830	14.8	10.4	-18.0	-27.7	a	95	360	54	Y
16 11 13.95	-20 19 18.9	56830	14.8	10.4	-9.7	-24.3	a	97	360	53	Y
16 16 23.53	-28 03 24.1	56830	14.7	11.3	-8.3	-23.7	b		360	37	
16 25 32.74	-26 11 38.6	56830	14.8	11.0	-17.7	-31.1	b		360	34	Y
16 26 49.58	-27 32 06.9	56830	14.8	9.8	0.5	-14.8	a	6	360	108	
16 32 35.87	-16 12 57.8	56830	14.8	9.6	-8.3	-13.1	b		360	86	Y
16 26 19.98	-22 58 10.0	56830	14.8	10.5	-4.8	-18.9	a	92	360	66	Y
16 10 39.79	-20 37 09.5	56830	14.9	9.9	-6.2	-24.9	a	90	360	62	Y
16 15 47.33	-19 11 18.5	56830	14.9	9.7	-6.9	-22.0	a	88	360	74	Y
16 13 38.35	-21 58 52.0	56830	14.9	11.0	-5.3	-24.7	a	73	360	46	Y
16 15 06.20	-25 00 46.1	56830	14.9	10.1	-16.1	-22.7	a	88	360	34	Y
16 23 55.10	-23 30 40.0	56830	14.9	10.1	-2.1	-27.7	a	74	360	74	Y
16 33 42.69	-22 24 39.7	56830	14.9	10.1	-1.4	-13.8	a	35	360	110	
16 28 46.05	-27 11 57.4	56830	14.9	10.4	-14.7	-24.6	a	97	360	80	Y
16 15 32.20	-20 10 23.7	56830	14.8	8.9	-6.1	-27.2	b		360	82	Y
16 33 35.04	-27 15 44.9	56830	15.0	11.0	-12.1	-21.0	a	95	360	62	Y
16 30 08.79	-24 32 29.4	56830	15.0	9.7	-7.8	-13.8	b		360	116	
16 19 43.10	-22 16 17.6	56830	15.0	11.3	-16.3	-19.7	b		360	41	Y
16 28 07.37	-20 17 47.8	56830	15.0	10.1	-13.3	-10.7	a	56	360	88	
16 17 06.08	-22 25 41.2	56830	15.0	11.2	-6.2	-22.4	a	53	360	31	Y
16 21 59.76	-27 06 36.6	56830	15.0	11.3	-8.7	-16.0	b		360	38	Y
16 25 48.09	-21 54 19.5	56830	15.0	11.2	-19.4	-24.7	b		360	24	Y
16 02 14.89	-24 38 32.6	56830	15.0	11.2	-19.8	-34.5	b		360	24	Y
16 03 54.05	-25 09 39.4	56830	15.0	11.4	-10.4	-33.4	b		360	28	Y
16 02 44.48	-25 43 32.3	56830	15.0	11.3	-13.0	-25.2	b		360	32	Y
16 21 29.62	-21 29 03.8	56830	14.9	11.2	-4.9	-22.2	b		360	26	Y
16 13 10.09	-24 35 24.8	56830	14.8	11.0	-9.8	-26.0	b		360	30	Y
16 04 39.66	-26 03 08.4	56830	14.7	11.4	-0.1	-30.2	b		360	58	
16 09 00.52	-27 45 19.4	56830	14.8	11.2	-20.9	-34.8	b		360	14	Y
16 27 06.69	-26 07 31.1	56831	10.1	8.3	-10.7	-17.1	b		300	149	
16 28 24.95	-27 23 18.4	56831	10.5	8.0	-10.0	-20.7	a	31	300	104	
16 12 43.73	-26 00 17.3	56831	11.0	8.1	-9.7	-20.7	b		300	17	
16 37 19.34	-28 44 04.5	56831	14.0	10.7	-8.1	-18.6	b		300	39	
16 18 43.89	-28 10 26.1	56831	14.0	11.1	-8.5	-12.4	b		300	60	
16 27 22.90	-19 46 48.5	56831	14.0	11.3	-5.3	-15.5	b		300	34	
16 23 43.51	-26 25 37.5	56831	14.0	10.8	-10.1	-28.5	b		300	28	
16 42 26.59	-28 27 35.2	56831	14.0	10.3	-11.5	-9.8	a	31	300	71	
16 51 24.97	-18 57 18.5	56831	14.0	11.1	-12.4	-30.8	b		300	67	
16 33 20.41	-15 34 14.2	56831	14.0	11.3	-16.3	-28.3	b		300	81	
16 33 51.15	-18 14 46.9	56831	14.0	11.3	-3.3	-36.5	b		300	68	
16 24 26.67	-27 20 10.2	56831	14.0	11.2	-15.9	-29.8	b		300	79	
16 35 45.74	-27 11 16.6	56831	14.0	10.3	-11.4	-24.2	a	97	300	60	Y
16 43 20.75	-28 34 40.5	56831	14.0	10.5	-5.8	-11.4	a	44	300	70	
16 24 43.85	-28 15 01.6	56831	14.0	10.1	-4.2	-16.2	a	18	180	68	
16 24 08.98	-26 22 40.4	56831	14.0	11.1	-14.7	-21.5	b		180	63	
16 37 48.40	-28 10 26.3	56831	14.0	11.2	-4.8	-20.4	b		180	69	
16 40 43.44	-27 39 18.4	56831	14.0	11.2	0.9	-24.3	b		180	70	

Continued on next page

Table 1. Summary of WiFeS observations of candidate Upper-Scorpius members; the V magnitude provided is either taken from APASS, where available, or interpolated from J and K according to the Kepler K2 instructions.

R.A. (J2000.0)	Decl. (J2000.0)	MJD	V (mag)	K (mag)	μ_α (mas)	μ_δ (mas)	Source	P_{mem}	T (sec)	SNR	M?
16 48 19.08	-24 57 50.6	56831	14.0	10.3	-6.4	-10.5	a	30	180	91	
16 28 16.09	-20 13 04.7	56831	14.0	11.1	-2.2	-27.4	b		180	63	
16 37 01.77	-15 57 01.9	56831	14.0	11.2	1.6	-19.8	b		180	60	
16 49 06.64	-24 06 13.2	56831	14.1	10.8	3.9	-20.8	a	27	180	51	
16 31 39.52	-28 42 18.0	56831	14.1	10.1	-0.1	-30.3	a	1	180	43	
16 36 20.68	-28 12 18.0	56831	14.0	9.5	-2.8	-16.8	a	55	180	19	

Table 2. Properties of the Upper Scorpius members identified in our survey. The first column lists our adopted naming system for these new members, and the second column lists the 2MASS designation for each of our targets. We also list the the fitted spectral type and visual extinction, and the equivalent widths of the Li 6708Å and Hα lines (EW(Li) and EW(Hα)). **The final star RIK-257, or HD 145788, is marked with an [a], is a likely disk-bearing F4.5-type members with some minimal Lithium absorption.**

Name	2MASS	R.A. (J2000.0)	Decl. (J2000.0)	EW(Li) (Å)	$\sigma_{EW(Li)}$ (Å)	EW(Hα) (Å)	$\sigma_{\rm EW(Li)}$ (Å)	A_V SpT	(mag)
RIK-1	J15390696-2646320	15 39 06.96	-26 46 32.1	0.46	0.02	-1.22	0.03	M0.5	0.2
RIK-2	J15413121-2520363	15 41 31.21	-25 20 36.3	0.40	0.01	-2.70	0.04	K2.5	0.1
RIK-3	J15422621-2247458	15 42 26.21	-22 47 46.0	0.46	0.04	-3.08	0.07	M1.5	0.3
RIK-4	J15450970-2512430	15 45 09.71	-25 12 43.0	0.61	0.02	-2.02	0.04	M1.5	0.4
RIK-5	J15471063-1736244	15 47 10.63	-17 36 24.3	0.52	0.05	-4.20	0.08	M2.0	0.2
RIK-6	J15474331-1819153	15 47 43.31	-18 19 15.4	0.55	0.02	-1.82	0.04	M1.5	0.0
RIK-7	J15492100-2600062	15 49 21.00	-26 00 06.3	0.44	0.02	-0.09	0.02	K4.5	0.1
RIK-8	J15492508-2843527	15 49 25.09	-28 43 52.8	0.54	0.03	-2.39	0.05	M2.0	0.0
RIK-9	J15530683-2247174	15 53 06.83	-22 47 17.4	0.66	0.03	-4.28	0.06	M1.0	0.7
RIK-10	J15540358-2920154	15 54 03.57	-29 20 15.6	0.46	0.03	-1.75	0.04	M1.5	0.0
RIK-11	J15550213-2149434	15 55 02.14	-21 49 43.5	0.48	0.02	-0.46	0.03	M0.0	0.3
RIK-12	J15550513-2026077	15 55 05.13	-20 26 07.7	0.40	0.02	-6.85	0.05	M2.5	0.8
RIK-13	J15550852-2318510	15 55 08.53	-23 18 51.1	0.55	0.01	-8.07	0.04	M1.5	0.7
RIK-14	J15552980-2544499	15 55 29.81	-25 44 50.0	0.53	0.02	-1.79	0.04	M0.5	0.9
RIK-15	J15553928-2053071	15 55 39.28	-20 53 07.3	0.81	0.04	-6.91	0.07	M4.0	1.0
RIK-16	J15554141-2043150	15 55 41.41	-20 43 15.1	0.64	0.01	-6.10	0.04	M1.0	0.6
RIK-17	J15555098-2519393	15 55 50.98	-25 19 39.4	0.60	0.03	-5.05	0.11	M4.5	0.0
RIK-18	J15561216-2354076	15 56 12.17	-23 54 07.7	0.36	0.08	-8.44	0.08	M5.0	0.4
RIK-19	J15562060-2336099	15 56 20.60	-23 36 10.0	0.45	0.02	-4.63	0.05	M3.5	0.5
RIK-20	J15562491-2541202	15 56 24.92	-25 41 20.3	0.27	0.02	-5.67	0.04	M3.0	0.3
RIK-21	J15562511-2016159	15 56 25.11	-20 16 15.8	0.61	0.07	-10.16	0.08	M5.0	1.0
RIK-22	J15563425-2003332	15 56 34.26	-20 03 33.3	0.63	0.06	-12.93	0.35	M5.5	0.8
RIK-23	J15564244-2039339	15 56 42.45	-20 39 34.2	0.54	0.02	-3.76	0.10	M3.5	0.6
RIK-24	J15564769-1950077	15 56 47.69	-19 50 07.6	0.60	0.02	-3.12	0.03	M2.0	0.3
RIK-25	J15565545-2258403	15 56 55.46	-22 58 40.4	0.58	0.04	-3.10	0.15	M0.5	0.1
RIK-26	J15570368-2304484	15 57 03.69	-23 04 48.3	0.68	0.02	-9.64	0.05	M4.5	0.8
RIK-27	J15571674-2529192	15 57 16.74	-25 29 19.3	0.67	0.04	-2.44	0.07	M0.0	0.3
RIK-28	J15572391-2051453	15 57 23.92	-20 51 45.4	0.60	0.02	-5.06	0.05	M2.5	0.7
RIK-29	J15572454-2038382	15 57 24.55	-20 38 38.2	0.52	0.04	-3.48	0.09	M1.5	0.0
RIK-30	J15573430-2321123	15 57 34.31	-23 21 12.3	0.58	0.02	-6.37	0.06	M1.0	0.5
RIK-31	J15574247-2551354	15 57 42.47	-25 51 35.6	0.59	0.06	-9.58	0.10	M4.5	0.7
RIK-32	J15580639-2340417	15 58 06.40	-23 40 41.9	0.44	0.03	-3.46	0.11	M3.5	0.8
RIK-33	J15580694-2623466	15 58 06.94	-26 23 46.7	0.44	0.02	-5.24	0.04	M2.5	0.4
RIK-34	J15581270-2328364	15 58 12.70	-23 28 36.4	0.25	0.01	0.89	0.02	K2.0	0.0
RIK-35	J15581571-2021368	15 58 15.73	-20 21 36.8	0.35	0.07	-9.36	0.31	M5.0	0.4
RIK-36	J15581884-1915448	15 58 18.85	-19 15 44.9	0.53	0.02	-3.81	0.04	M1.5	0.7
RIK-37	J15582855-2334190	15 58 28.56	-23 34 19.1	0.42	0.02	-5.07	0.13	M3.5	0.5
RIK-38	J15583620-1946135	15 58 36.20	-19 46 13.5	0.70	0.04	-4.02	0.10	M4.0	0.6
RIK-39	J15585820-2304352	15 58 58.21	-23 04 35.2	0.60	0.03	-7.71	0.19	M1.5	0.4
RIK-40	J15590193-2616329	15 59 01.93	-26 16 33.0	0.57	0.08	-10.57	0.61	M5.5	0.3
RIK-41	J15590864-2600545	15 59 08.65	-26 00 54.4	0.49	0.05	-7.27	0.35	M3.5	0.0
RIK-42	J15593807-2603233	15 59 38.07	-26 03 23.5	0.81	0.08	-16.24	0.11	M5.5	0.7
RIK-43	J15594426-2029232	15 59 44.27	-20 29 23.4	0.69	0.19	-10.95	0.86	M5.0	0.6
RIK-44	J15595270-2526292	15 59 52.69	-25 26 29.2	0.48	0.04	-2.01	0.09	M0.5	0.3
RIK-45	J15595995-2220367	15 59 59.95	-22 20 36.8	0.59	0.03	-4.64	0.05	M1.0	0.6
RIK-46	J16000704-2340487	16 00 07.05	-23 40 48.7	0.61	0.04	-20.54	0.16	M5.5	0.6
RIK-47	J16001216-2157032	16 00 12.17	-21 57 03.3	0.43	0.03	-4.37	0.14	M2.5	0.0
RIK-48	J16001330-2418106	16 00 13.30	-24 18 10.7	0.59	0.03	-2.14	0.04	M0.5	0.4
RIK-49	J16004056-2200322	16 00 40.56	-22 00 32.2	0.42	0.01	0.28	0.02	K4.0	0.0
RIK-50	J16004277-2127380	16 00 42.77	-21 27 38.0	0.55	0.02	-2.37	0.04	M0.0	0.1
RIK-51	J16004309-2430503	16 00 43.10	-24 30 50.5	0.38	0.06	-10.46	1.23	M4.5	0.2
RIK-52	J16004973-2338432	16 00 49.73	-23 38 43.2	0.60	0.02	-4.16	0.04	M1.5	0.7
RIK-53	J16004989-1928003	16 00 49.89	-19 28 00.4	0.61	0.06	-5.38	0.18	M1.5	0.7
RIK-54	J16005271-2523426	16 00 52.72	-25 23 42.7	0.46	0.07	-4.11	0.10	M3.0	0.0

Continued on next page

RIK-55	J16010896-2645104	16 01 08.97	-26 45 10.6	0.47	0.05	-5.38	0.19	M3.5	0.0
RIK-56	J16011398-2516281	16 01 13.99	-25 16 28.2	0.48	0.04	-5.88	0.15	M4.0	0.0
RIK-57	J16012233-1937222	16 01 22.34	-19 37 22.3	0.45	0.02	-2.59	0.03	M1.5	0.7
RIK-58	J16012902-2509069	16 01 29.03	-25 09 06.9	0.34	0.03	-129.46	13.94	M3.5	0.3
RIK-59	J16015987-1843457	16 01 59.88	-18 43 45.7	0.36	0.02	-4.25	0.10	M2.5	0.9
RIK-60	J16020039-2221237	16 02 00.39	-22 21 23.9	0.66	0.04	-4.23	0.05	M1.0	0.7
RIK-61	J16020845-2254588	16 02 08.45	-22 54 59.1	0.67	0.03	-3.50	0.05	M1.0	0.6
RIK-62	J16021489-2438325	16 02 14.89	-24 38 32.6	0.66	0.09	-15.33	0.46	M5.5	0.7
RIK-63	J16022357-2259332	16 02 23.57	-22 59 33.3	0.49	0.09	-13.91	1.23	M6.0	1.0
RIK-64	J16022461-2200248	16 02 24.61	-22 00 24.8	0.72	0.04	-3.92	0.07	M1.5	0.0
RIK-65	J16023587-2320170	16 02 35.89	-23 20 17.1	0.53	0.03	-8.46	1.34	M3.5	0.6
RIK-66	J16024448-2543323	16 02 44.48	-25 43 32.3	0.45	0.04	-8.79	1.50	M4.0	0.0
RIK-67	J16030177-2626218	16 03 01.77	-26 26 21.9	0.46	0.03	-2.95	0.15	M0.0	0.0
RIK-68	J16031491-2234454	16 03 14.91	-22 34 45.5	0.48	0.05	-15.50	9.06	M4.5	0.3
RIK-69	J16032599-2627320	16 03 25.98	-26 27 32.2	0.83	0.07	-9.27	0.11	M4.5	0.4
RIK-70	J16033777-1845083	16 03 37.77	-18 45 08.3	0.56	0.04	-4.65	0.08	M1.0	0.5
RIK-71	J16033829-1854076	16 03 38.30	-18 54 07.7	0.55	0.02	-4.37	0.04	M1.0	0.8
RIK-72	J16033922-1851294	16 03 39.22	-18 51 29.3	0.59	0.03	-2.28	0.14	M2.5	0.6
RIK-73	J16034695-2245246	16 03 46.95	-22 45 24.7	0.42	0.04	-3.86	0.31	M1.5	0.0
RIK-74	J16035175-2140154	16 03 51.75	-21 40 15.5	0.55	0.04	-14.20	0.64	M6.0	0.7
RIK-75	J16035404-2509393	16 03 54.05	-25 09 39.4	0.59	0.06	-7.55	0.32	M5.5	0.2
RIK-76	J16040671-2637070	16 04 06.71	-26 37 07.1	0.52	0.03	-4.27	0.04	M1.5	0.6
RIK-77	J16041893-2430392	16 04 18.93	-24 30 39.3	0.57	0.02	-24.08	0.37	M2.5	0.3
RIK-78	J16052157-1821412	16 05 21.57	-18 21 41.2	0.47	0.02	-37.96	0.15	K4.5	1.0
RIK-79	J16053815-2039469	16 05 38.16	-20 39 47.0	0.59	0.02	-1.09	0.03	M0.0	0.3
RIK-80	J16064385-1908056	16 06 43.86	-19 08 05.5	0.59	0.02	-8.57	0.07	M0.0	0.6
RIK-81	J16064794-1841437	16 06 47.94	-18 41 43.8	0.49	0.02	-0.92	0.04	M0.0	0.3
RIK-82	J16071403-1702425	16 07 14.02	-17 02 42.7	0.71	0.04	-3.70	0.09	M3.5	0.7
RIK-83	J16073037-2546269	16 07 30.38	-25 46 27.0	0.44	0.01	-2.82	0.03	M1.5	0.5
RIK-84	J16074006-2148426	16 07 40.06	-21 48 42.7	0.51	0.02	-2.06	0.05	M0.5	0.3
RIK-85	J16075136-1718231	16 07 51.37	-17 18 23.2	0.54	0.03	-4.09	0.04	M2.5	0.6
RIK-86	J16080141-2027416	16 08 01.42	-20 27 41.7	0.62	0.08	-1.93	0.18	M0.0	0.9
RIK-87	J16080411-2640449	16 08 04.11	-26 40 44.9	0.47	0.06	-7.81	0.54	M0.5	0.0
RIK-88	J16082078-2131234	16 08 20.77	-21 31 23.4	0.70	0.04	-5.62	0.19	M4.5	0.7
RIK-89	J16085628-2148489	16 08 56.29	-21 48 48.9	0.56	0.02	-3.71	0.03	M1.5	0.5
RIK-90	J16085695-2835573	16 08 56.96	-28 35 57.4	0.21	0.06	-10.18	0.18	M4.5	0.9
RIK-91	J16090051-2745194	16 09 00.52	-27 45 19.4	0.80	0.18	-11.25	0.62	M5.5	1.1
RIK-92	J16092063-2222057	16 09 20.63	-22 22 05.7	0.56	0.08	-16.49	0.39	M5.5	0.8
RIK-93	J16092969-2200579	16 09 29.70	-22 00 58.0	0.59	0.02	-3.34	0.03	M1.5	0.7
RIK-94	J16093030-2104589	16 09 30.31	-21 04 58.9	0.49	0.02	-0.76	0.03	M0.0	0.3
RIK-95	J16093108-2041460	16 09 31.10	-20 41 46.0	0.53	0.03	-9.06	0.06	M4.5	1.0
RIK-96	J16093164-2229224	16 09 31.66	-22 29 22.4	0.38	0.07	-4.90	0.10	M2.0	0.9
RIK-97	J16093575-2138057	16 09 35.76	-21 38 05.8	0.55	0.01	-3.66	0.03	M2.5	0.7
RIK-98	J16093969-2200466	16 09 39.70	-22 00 46.6	0.51	0.03	-3.00	0.08	M0.5	0.7
RIK-99	J16094955-2444468	16 09 49.55	-24 44 46.8	0.55	0.01	-4.75	0.11	M1.5	0.4
RIK-100	J16095287-2441535	16 09 52.88	-24 41 53.6	0.51	0.06	-15.07	0.44	M5.5	0.9
RIK-101	J16100394-2728479	16 10 03.94	-27 28 48.0	0.64	0.05	-7.64	0.19	M4.5	0.8
RIK-102	J16100501-2132318	16 10 05.02	-21 32 31.9	0.43	0.02	-54.01	1.71	M0.0	0.3
RIK-103	J16101445-1951377	16 10 14.46	-19 51 37.5	0.63	0.02	-4.90	0.04	M4.0	0.6
RIK-104	J16102625-2209105	16 10 26.25	-22 09 10.5	0.60	0.03	-7.54	0.05	M3.5	0.7
RIK-105	J16103978-2037094	16 10 39.79	-20 37 09.5	0.63	0.02	-4.87	0.35	M2.5	0.9
RIK-106	J16110479-2333166	16 11 04.80	-23 33 16.6	0.39	0.04	-1.88	0.13	M0.0	0.0
RIK-107	J16110567-2144032	16 11 05.67	-21 44 03.3	0.63	0.02	-6.01	0.04	M1.5	0.9
RIK-108	J16111395-2019188	16 11 13.95	-20 19 18.9	0.65	0.04	-12.08	0.36	M3.5	0.8
RIK-109	J16111687-2639331	16 11 16.87	-26 39 33.1	0.60	0.05	-5.85	0.20	M5.0	0.5
RIK-110	J16111744-2441203	16 11 17.45	-24 41 20.4	0.63	0.02	-5.77	0.04	M4.0	0.4
RIK-111	J16112601-2631558	16 11 26.03	-26 31 55.9	0.54	0.05	-3.59	0.10	M2.0	0.7
RIK-112	J16120505-2043404	16 12 05.05	-20 43 40.5	0.57	0.03	-12.34	0.20	M1.0	1.2
RIK-113	J16120668-3010270	16 12 06.68	-30 10 27.1	0.55	0.03	-33.77	0.14	M0.5	0.2
RIK-114	J16120814-2547578	16 12 08.14	-25 47 57.9	0.66	0.03	-6.59	0.07	M3.5	0.6

Continued on next page

RIK-115	J16121368-2431369	16 12 13.69	-24 31 36.9	0.31	0.03	-4.25	0.05	M2.5	0.6
RIK-116	J16121723-2839082	16 12 17.24	-28 39 08.6	0.61	0.06	-7.14	0.58	M4.5	0.2
RIK-117	J16123352-2543281	16 12 33.54	-25 43 27.6	0.69	0.06	-8.52	0.22	M4.0	0.6
RIK-118	J16123531-2034339	16 12 35.32	-20 34 34.0	0.46	0.03	-2.30	0.07	M0.5	0.8
RIK-119	J16123604-2723031	16 12 36.05	-27 23 03.2	0.39	0.03	1.06	0.03	K4.0	1.2
RIK-120	J16130627-2606107	16 13 06.28	-26 06 10.7	0.38	0.03	-6.11	0.07	M3.5	0.7
RIK-121	J16130978-2044591	16 13 09.79	-20 44 59.1	0.57	0.03	-6.11	0.04	M3.5	0.9
RIK-122	J16131008-2435248	16 13 10.09	-24 35 24.8	0.65	0.06	-7.67	0.33	M4.5	1.0
RIK-123	J16132054-2229159	16 13 20.55	-22 29 15.9	0.38	0.02	-4.18	0.07	M1.5	0.4
RIK-124	J16132190-2136136	16 13 21.91	-21 36 13.7	0.53	0.03	-21.99	0.20	M1.5	0.2
RIK-125	J16133279-2044413	16 13 32.79	-20 44 41.4	0.48	0.02	-1.96	0.03	M2.5	0.8
RIK-126	J16133644-2326270	16 13 36.44	-23 26 27.0	0.36	0.02	-5.87	0.04	M2.5	0.4
RIK-127	J16133834-2158518	16 13 38.35	-21 58 52.0	0.43	0.04	-4.62	0.12	M4.5	0.8
RIK-128	J16133840-2443309	16 13 38.40	-24 43 31.2	0.33	0.02	-10.56	0.07	M3.5	0.6
RIK-129	J16134490-2434143	16 13 44.90	-24 34 14.4	0.47	0.02	-7.23	0.05	M2.5	0.7
RIK-130	J16135663-2457566	16 13 56.62	-24 57 56.8	0.36	0.02	-5.08	0.04	M3.5	0.7
RIK-131	J16140380-2453088	16 14 03.80	-24 53 08.9	0.42	0.02	-2.48	0.06	M1.0	0.6
RIK-132	J16140733-2217321	16 14 07.35	-22 17 32.2	0.57	0.05	-4.97	0.18	M1.0	0.0
RIK-133	J16141011-2217236	16 14 10.12	-22 17 23.5	0.62	0.04	-3.09	0.04	M4.0	0.7
RIK-134	J16141259-2454287	16 14 12.58	-24 54 28.8	0.49	0.02	-2.06	0.03	M0.5	0.6
RIK-135	J16143363-2004299	16 14 33.64	-20 04 29.9	0.55	0.02	-4.44	0.08	M3.5	0.6
RIK-136	J16144125-2556052	16 14 41.26	-25 56 05.3	0.67	0.02	-3.99	0.05	M1.5	0.7
RIK-137	J16144989-2139321	16 14 49.89	-21 39 32.2	0.56	0.02	-2.61	0.03	M2.5	0.4
RIK-138	J16145244-2513523	16 14 52.41	-25 13 52.4	0.16	0.03	-6.54	0.50	M3.5	0.6
RIK-139	J16145269-2308025	16 14 52.70	-23 08 02.7	0.42	0.03	-4.23	0.04	M3.5	0.6
RIK-140	J16150060-2919348	16 15 00.60	-29 19 34.9	0.28	0.03	-3.54	0.09	M3.0	0.2
RIK-141	J16150620-2500459	16 15 06.20	-25 00 46.1	0.56	0.05	-8.56	0.47	M4.5	1.3
RIK-142	J16151104-2322425	16 15 11.05	-23 22 42.7	0.56	0.03	-3.39	0.03	M1.0	0.4
RIK-143	J16151239-2318453	16 15 12.40	-23 18 45.3	0.30	0.05	-1.15	0.11	K6.0	0.0
RIK-144	J16151948-2540119	16 15 19.49	-25 40 12.0	0.66	0.04	-7.58	0.14	M1.5	0.7
RIK-145	J16152750-2627281	16 15 27.51	-26 27 28.1	0.46	0.04	-4.09	0.06	M4.0	1.0
RIK-146	J16153220-2010236	16 15 32.20	-20 10 23.7	0.60	0.02	-11.06	0.15	M1.5	1.0
RIK-147	J16153311-2707587	16 15 33.11	-27 07 58.8	0.58	0.03	-2.55	0.06	M0.5	0.6
RIK-148	J16153587-2529008	16 15 35.86	-25 29 01.0	0.41	0.02	-0.13	0.02	K4.5	0.7
RIK-149	J16153642-2622090	16 15 36.43	-26 22 09.2	0.36	0.03	-4.29	0.08	M3.5	0.0
RIK-150	J16154732-1911184	16 15 47.33	-19 11 18.5	0.57	0.02	-5.08	0.12	M1.5	1.2
RIK-151	J16155987-2325043	16 15 59.86	-23 25 04.5	0.49	0.03	-0.80	0.04	M0.0	0.0
RIK-152	J16160080-2214192	16 16 00.81	-22 14 19.3	0.51	0.04	-9.47	0.33	M5.5	0.1
RIK-153	J16160292-2430548	16 16 02.92	-24 30 54.8	0.47	0.05	-1.92	0.07	M1.0	0.8
RIK-154	J16160856-2041514	16 16 08.55	-20 41 51.5	0.56	0.03	-3.81	0.10	M4.0	0.6
RIK-155	J16160947-2243437	16 16 09.48	-22 43 43.8	0.39	0.02	-4.15	0.04	M1.5	0.5
RIK-156	J16161720-2609101	16 16 17.20	-26 09 10.2	0.71	0.05	-2.24	0.06	K4.0	0.3
RIK-157	J16161893-2542287	16 16 18.94	-25 42 28.7	0.61	0.04	-7.34	0.14	M1.5	0.7
RIK-158	J16163346-2552367	16 16 33.45	-25 52 36.8	0.53	0.02	-2.84	0.04	M0.5	1.3
RIK-159	J16165130-2433277	16 16 51.30	-24 33 27.7	0.14	0.02	3.59	0.06	F8.0	1.4
RIK-160	J16165984-2154272	16 16 59.84	-21 54 27.3	0.17	0.02	-4.22	0.05	M3.5	0.4
RIK-161	J16170606-2225414	16 17 06.08	-22 25 41.2	0.31	0.04	-4.78	0.18	M4.5	0.9
RIK-162	J16171380-2251584	16 17 13.80	-22 51 58.5	0.58	0.04	-7.15	0.20	M4.5	0.4
RIK-163	J16171649-2327570	16 17 16.50	-23 27 57.1	0.61	0.02	-8.59	0.05	M3.5	0.6
RIK-164	J16172162-2325004	16 17 21.63	-23 25 00.4	0.64	0.03	-2.00	0.07	M4.0	0.5
RIK-165	J16172297-2121119	16 17 22.98	-21 21 11.9	0.60	0.02	-1.45	0.05	M1.0	0.0
RIK-166	J16172615-2450592	16 17 26.15	-24 50 59.2	0.45	0.02	-5.71	0.04	M2.5	1.3
RIK-167	J16172769-2421025	16 17 27.70	-24 21 02.6	0.55	0.04	-7.42	0.66	M4.5	0.6
RIK-168	J16172994-2451030	16 17 29.95	-24 51 03.2	0.34	0.02	-6.97	0.04	M2.5	1.4
RIK-169	J16173031-2438390	16 17 30.32	-24 38 39.2	0.58	0.03	-1.72	0.05	M0.0	1.6
RIK-170	J16173138-2303360	16 17 31.38	-23 03 36.0	0.24	0.02	1.05	0.03	K1.5	0.0
RIK-171	J16175501-2711303	16 17 55.02	-27 11 30.4	0.46	0.02	-2.95	0.04	M1.5	0.2
RIK-172	J16181997-2005348	16 18 19.98	-20 05 34.9	0.33	0.03	1.24	0.04	K1.5	0.4
RIK-173	J16190214-2138097	16 19 02.15	-21 38 09.7	0.43	0.02	-6.13	0.05	M4.5	0.2
RIK-174	J16191473-2532314	16 19 14.74	-25 32 31.3	0.34	0.02	0.59	0.02	K4.5	0.7

Continued on next page

RIK-175	J16191608-2915126	16 19 16.09	-29 15 12.7	0.52	0.02	-4.94	0.04	M4.0	0.2
RIK-176	J16193139-2518127	16 19 31.39	-25 18 12.8	0.40	0.03	0.45	0.04	K6.0	0.9
RIK-177	J16194309-2216175	16 19 43.10	-22 16 17.6	0.69	0.05	-2.78	0.10	M4.5	0.5
RIK-178	J16194538-2147577	16 19 45.38	-21 47 57.8	0.35	0.03	-2.56	0.05	M1.5	0.0
RIK-179	J16194711-2203112	16 19 47.12	-22 03 11.2	0.49	0.04	-8.67	0.07	M5.0	0.5
RIK-180	J16194836-2212519	16 19 48.36	-22 12 51.8	0.43	0.03	-16.57	0.14	M3.0	0.3
RIK-181	J16194880-2224472	16 19 48.78	-22 24 47.5	0.88	0.06	-15.55	0.10	M6.0	0.3
RIK-182	J16194885-2140360	16 19 48.86	-21 40 36.0	0.57	0.04	-4.93	0.13	M4.5	0.1
RIK-183	J16200616-2212385	16 20 06.16	-22 12 38.5	0.60	0.03	-2.49	0.06	M3.5	0.2
RIK-184	J16200686-2247320	16 20 06.86	-22 47 32.1	0.52	0.04	-8.63	0.21	M4.5	0.9
RIK-185	J16202163-2005348	16 20 21.64	-20 05 34.8	1.07	0.25	-5.85	0.96	M7.5	2.8
RIK-186	J16202498-2150240	16 20 24.98	-21 50 23.9	0.47	0.02	-4.61	0.09	M2.0	0.2
RIK-187	J16202724-2126068	16 20 27.24	-21 26 06.9	0.52	0.04	-2.51	0.05	M1.5	0.0
RIK-188	J16203246-2257452	16 20 32.46	-22 57 45.4	0.51	0.01	-7.12	0.04	M2.5	1.4
RIK-189	J16203640-2123120	16 20 36.41	-21 23 12.0	0.65	0.04	-13.01	0.09	M4.5	0.5
RIK-190	J16204578-2849201	16 20 45.79	-28 49 20.1	0.66	0.07	-5.67	0.11	M2.0	0.3
RIK-191	J16205095-2253399	16 20 50.95	-22 53 40.1	0.49	0.02	-1.52	0.04	M1.0	1.5
RIK-192	J16211584-2240045	16 21 15.84	-22 40 04.5	0.53	0.02	-5.35	0.06	M1.5	0.9
RIK-193	J16212953-2529431	16 21 29.55	-25 29 43.1	0.29	0.02	-4.29	0.06	M2.5	0.7
RIK-194	J16212961-2129038	16 21 29.62	-21 29 03.8	0.93	0.09	-13.95	0.47	M5.5	0.8
RIK-195	J16214126-2212056	16 21 41.26	-22 12 05.5	0.54	0.04	-7.42	0.15	M4.5	0.5
RIK-196	J16214853-2517266	16 21 48.54	-25 17 26.6	0.48	0.01	-1.21	0.03	M0.0	1.4
RIK-197	J16215466-2043091	16 21 54.67	-20 43 09.1	0.38	0.05	-0.57	0.04	K7	0.0
RIK-198	J16215594-2705034	16 21 55.94	-27 05 03.4	0.61	0.04	-7.69	0.07	M5.0	0.3
RIK-199	J16215975-2706366	16 21 59.76	-27 06 36.6	0.51	0.06	-5.34	0.18	M4.5	0.3
RIK-200	J16220587-2121556	16 22 05.88	-21 21 55.6	0.30	0.01	-2.57	0.02	M1.5	0.6
RIK-201	J16220658-2127089	16 22 06.59	-21 27 08.9	0.53	0.02	-7.31	0.05	M3.5	0.5
RIK-202	J16220858-2915063	16 22 08.59	-29 15 06.4	0.61	0.03	-3.40	0.08	M2.5	0.2
RIK-203	J16220894-2140372	16 22 08.94	-21 40 37.2	0.39	0.03	-4.48	0.06	M3.5	0.5
RIK-204	J16222092-2747095	16 22 20.93	-27 47 09.6	0.58	0.02	-3.88	0.04	M2.5	0.2
RIK-205	J16224408-2142222	16 22 44.07	-21 42 22.2	0.53	0.04	-3.36	0.05	M3.5	0.6
RIK-206	J16225479-2138091	16 22 54.78	-21 38 09.3	0.31	0.01	-5.52	0.04	M2.5	0.7
RIK-207	J16230474-2759252	16 23 04.74	-27 59 25.4	0.37	0.01	-1.83	0.02	M0.0	0.6
RIK-208	J16231741-2159067	16 23 17.41	-21 59 07.0	0.61	0.03	-5.03	0.35	M3.5	0.6
RIK-209	J16232293-2622161	16 23 22.93	-26 22 16.1	0.15	0.04	1.92	0.11	F5.0	0.0
RIK-210	J16232454-1717270	16 23 24.54	-17 17 27.1	0.59	0.02	-5.29	0.09	M2.5	0.3
RIK-211	J16233234-2523485	16 23 32.34	-25 23 48.5	0.31	0.01	0.22	0.01	K2.0	1.3
RIK-212	J16235509-2330396	16 23 55.10	-23 30 40.0	0.53	0.02	-3.48	0.08	M2.5	1.2
RIK-213	J16235723-2620244	16 23 57.23	-26 20 24.6	0.33	0.02	-7.36	0.05	M4.5	0.3
RIK-214	J16235790-2602296	16 23 57.91	-26 02 29.9	0.39	0.02	-1.01	0.03	M0.0	0.9
RIK-215	J16235902-2736037	16 23 59.02	-27 36 03.7	0.47	0.02	-6.44	0.04	M3.5	0.2
RIK-216	J16240942-2134075	16 24 09.43	-21 34 07.3	0.33	0.11	-5.41	0.30	M3.5	1.1
RIK-217	J16241177-1955583	16 24 11.77	-19 55 58.3	0.51	0.01	-4.78	0.04	M1.5	1.2
RIK-218	J16241551-2544344	16 24 15.52	-25 44 34.5	0.31	0.02	-0.04	0.02	M0.0	1.2
RIK-219	J16241860-2854475	16 24 18.60	-28 54 47.5	0.37	0.02	0.85	0.03	G8.5	1.3
RIK-220	J16250236-2321447	16 25 02.37	-23 21 45.1	0.65	0.03	-3.08	0.05	M1.0	1.8
RIK-221	J16251690-2322030	16 25 16.90	-23 22 03.6	0.63	0.03	-3.62	0.09	M0.0	1.9
RIK-222	J16252327-2727314	16 25 23.27	-27 27 31.5	0.49	0.03	-8.88	0.06	M5.0	0.2
RIK-223	J16252883-2607538	16 25 28.81	-26 07 53.8	0.55	0.02	-2.86	0.04	M2.5	0.9
RIK-224	J16253274-2611386	16 25 32.74	-26 11 38.6	0.72	0.06	-8.74	0.34	M5.5	0.8
RIK-225	J16253504-2332549	16 25 35.04	-23 32 55.0	0.58	0.03	-2.18	0.07	M0.0	2.1
RIK-226	J16254808-2154195	16 25 48.09	-21 54 19.5	0.42	0.06	-4.53	0.42	M3.5	0.2
RIK-227	J16254925-2554371	16 25 49.24	-25 54 37.3	0.47	0.02	-1.40	0.03	M0.0	1.2
RIK-228	J16255541-2721242	16 25 55.41	-27 21 24.3	0.73	0.04	-8.91	0.23	M5.0	0.1
RIK-229	J16255790-2600374	16 25 57.91	-26 00 37.3	0.31	0.06	-0.14	0.08	G8.0	1.3
RIK-230	J16261964-2137207	16 26 19.64	-21 37 20.8	0.43	0.02	-1.07	0.03	M1.5	0.8
RIK-231	J16261998-2233023	16 26 19.98	-22 33 02.5	0.48	0.03	-1.24	0.04	M1.5	0.8
RIK-232	J16261995-2258097	16 26 19.98	-22 58 10.0	0.60	0.03	-3.06	0.07	M3.5	0.7
RIK-233	J16262016-2233124	16 26 20.16	-22 33 12.7	0.34	0.04	-4.53	0.09	M3.5	0.8
RIK-234	J16262803-2526477	16 26 28.04	-25 26 47.8	0.52	0.02	-2.00	0.03	M0.0	1.8

Continued on next page

RIK-235	J16263276-2622589	16 26 32.77	-26 22 59.0	0.58	0.12	-5.88	0.53	M6.0	1.2
RIK-236	J16263495-2511409	16 26 34.95	-25 11 40.9	0.48	0.01	-1.01	0.02	M0.0	1.1
RIK-237	J16264120-2200094	16 26 41.21	-22 00 09.5	0.35	0.02	-2.80	0.08	M1.5	0.7
RIK-238	J16270950-2618549	16 27 09.51	-26 18 54.9	0.48	0.04	-8.58	0.10	M4.5	0.5
RIK-239	J16271273-2504017	16 27 12.74	-25 04 01.8	0.53	0.02	-9.14	0.12	M1.0	0.9
RIK-240	J16272766-2821502	16 27 27.66	-28 21 50.4	0.56	0.03	-5.38	0.15	M2.0	0.3
RIK-241	J16273320-2821097	16 27 33.22	-28 21 09.8	0.13	0.01	-4.93	0.05	M3.5	0.2
RIK-242	J16275794-2524187	16 27 57.93	-25 24 18.8	0.32	0.03	-6.06	0.13	M3.5	0.1
RIK-243	J16284604-2711574	16 28 46.05	-27 11 57.4	0.33	0.02	-2.52	0.08	M1.5	1.1
RIK-244	J16295662-2659182	16 29 56.63	-26 59 18.4	0.52	0.03	-8.00	0.08	M4.5	0.1
RIK-245	J16300275-2727006	16 30 02.76	-27 27 00.5	0.42	0.04	-3.65	0.19	M1.5	0.1
RIK-246	J16310579-2725460	16 31 05.80	-27 25 46.1	0.38	0.04	-9.05	0.11	M4.5	0.3
RIK-247	J16311542-2657151	16 31 15.42	-26 57 15.1	0.45	0.02	-2.12	0.06	M1.5	0.7
RIK-248	J16315668-2846126	16 31 56.69	-28 46 12.7	0.17	0.04	-9.99	0.10	M4.0	0.7
RIK-249	J16323587-1612577	16 32 35.87	-16 12 57.8	0.13	0.01	0.90	0.02	K4.5	2.3
RIK-250	J16333496-1832540	16 33 34.97	-18 32 53.9	0.17	0.05	-8.47	0.21	M3.5	0.4
RIK-251	J16333503-2715448	16 33 35.04	-27 15 44.9	0.35	0.03	-3.86	0.25	M3.5	0.4
RIK-252	J16333881-2150263	16 33 38.83	-21 50 26.3	0.73	0.02	-1.70	0.03	M1.5	1.3
RIK-253	J16343514-2658030	16 34 35.14	-26 58 03.1	0.54	0.05	-27.10	0.70	M4.5	0.5
RIK-254	J16343826-2835504	16 34 38.27	-28 35 50.5	0.22	0.02	-3.31	0.04	M1.0	0.8
RIK-255	J16350625-2025282	16 35 06.26	-20 25 28.3	0.61	0.04	-11.45	0.14	M4.5	0.6
RIK-256	J16354573-2711166	16 35 45.74	-27 11 16.6	0.26	0.02	-8.03	2.47	M1.5	0.0
RIK-257[a]	J16134781-2747340	16 13 47.82	-27 47 34.0	0.09	0.02	4.14	0.04	F4.5	0.2